A cell-based MAPK reporter assay reveals synergistic MAPK pathway activity suppression by MAPK inhibitor combination in *BRAF*-driven pediatric low-grade glioma cells

Diren Usta[1-3], Romain Sigaud[1,2], Juliane L. Buhl[1,2,4], Florian Selt[1-3], Viktoria Marquardt[5], David Pauck[5], Jennifer Jansen[6] Stefan Pusch[7,8], Jonas Ecker[1-3], Thomas Hielscher[9], Johanna Vollmer[1,2], Alexander C. Sommerkamp[1, 4, 10], Tobias Rubner[11], Darren Hargrave[12], Cornelis M. van Tilburg[1-3], Stefan M. Pfister[1,3,13], David T.W. Jones[1,10], Marc Remke[5], Tilman Brummer[6], Olaf Witt[1-3], Till Milde[1-3*]

[1] Hopp Children's Cancer Center Heidelberg (KiTZ), Heidelberg, Germany

[2] Clinical Cooperation Unit Pediatric Oncology, German Cancer Research Center (DKFZ) and German Consortium for Translational Cancer Research (DKTK), Heidelberg, Germany

[3] KiTZ Clinical Trial Unit (ZIPO), Department of Pediatric Hematology and Oncology, Heidelberg University Hospital, Heidelberg, Germany

[4] Faculty of Biosciences, Heidelberg University, Heidelberg, Germany

[5] Department of Pediatric Oncology, Hematology, and Clinical Immunology, Medical Faculty, University Hospital Düsseldorf, Germany, and Department of Pediatric Neuro-Oncogenomics, German Cancer Consortium (DKTK) and German Cancer Research Center (DKFZ), Heidelberg, Germany

[6] Institute of Molecular Medicine and Cell Research (IMMZ), Faculty of Medicine, University of Freiburg, Freiburg, Germany, Centre for Biological Signalling Studies BIOSS, University of Freiburg, Comprehensive Cancer Center Freiburg (CCCF) and German Consortium for Translational Cancer Research (DKTK), Freiburg, and German Cancer Research Center (DKFZ), Heidelberg, Germany

[7]Department of Neuropathology, Heidelberg University Hospital, Heidelberg, Germany

[8] Clinical Cooperation Unit Neuropathology, German Cancer Research Center (DKFZ) and German Consortium for Translational Cancer Research (DKTK), Heidelberg, Germany

[9] Division of Biostatistics, German Cancer Research Center (DKFZ) and German Consortium for Translational Cancer Research (DKTK), Heidelberg, Germany

[10] Pediatric Glioma Research Group, German Cancer Research Center (DKFZ), Heidelberg, Germany

[11] Flow Cytometry Unit, German Cancer Research Center (DKFZ), Heidelberg, Germany

[12] Neurooncology and Experimental Therapeutics, Great Ormond Street Hospital for Children, London, United Kingdom

[13] Division of Pediatric Neurooncology, German Cancer Research Center (DKFZ) and German Consortium for Translational Cancer Research (DKTK), Heidelberg, German

Running title: MAPK reporter assay in pediatric low-grade glioma cells

Keywords: pediatric pilocytic astrocytoma, BRAF inhibitor, MEK inhibitor, ERK inhibitor, ELK-1 reporter assay

Additional information:

Financial support, including the source and number of grants, for each author:
S.M. Pfister, D.T.W. Jones, and O. Witt received financial support from The Brain Tumour Charity (TBTC, The Everest Centre for Low-Grade Paediatric Brain Tumours; GN-000382). D. Usta received a scholarship from the Friedrich-Ebert-Foundation ("Friedrich-Ebert-Stiftung"). J. Vollmer received a scholarship from The German National Academic Foundation ("Studienstiftung des deutschen Volkes"). J. Ecker received a postdoc stipend from the Medical Faculty, Heidelberg University, through the Physician Scientist Program. T. Brummer acknowledges support by the German Research Foundation (DFG) by a Heisenberg-Professorship and BR3662/4–1. O. Witt is grateful to Christian Scheu and his family for their financial support of this study. S.M. Pfister, D.T.W. Jones, and O. Witt received financial support from A Kids' Brain Tumor Cure (PLGA Foundation). O. Witt, D.T.W. Jones and S.M. Pfister received financial support from Children's Tumor Foundation Synodos low-grade glioma initiative. O. Witt and T. Milde received donations from private charities (anonymous, "Verein für krebskranke Kinder Odenwald e.V." and the "DLFH Verband Pfalz e.V."). D. Hargrave is supported by funding from the NIHR Great Ormond Street Hospital Biomedical Research Centre. The views expressed are those of the author(s) and not necessarily those of the NHS, the NIHR or the Department of Health.

* Corresponding author:
Till Milde, Hopp Children's Cancer Center Heidelberg (KiTZ), Clinical Cooperation Unit Pediatric Oncology (B310), German Cancer Research Center (DKFZ), Im Neuenheimer Feld 280, 69120 Heidelberg, Germany; phone: +49 6221 42 3574, fax: +49 6221 3579, email: t.milde@kitz-heidelberg.de.

Disclosure of potential conflicts of interest:
C. van Tilburg participated at advisory boards of Novartis and Bayer. D. Hargrave has acted as a paid/unpaid consultant and advisor for selumetinib (AstraZeneca), cobimetinib (Roche) and trametinib/ dabrafenib (Novartis) and received research funding from AstraZeneca. O. Witt is advisory board member of Novartis, AstraZeneca, Janssen and Roche.

Word count: 6430

Total number of Figures: 6, Suppl. Figures: 5

Total number of Suppl. Tables: 5

Abstract

Pilocytic astrocytomas (PAs) as well as other pediatric low-grade gliomas (pLGGs) exhibit genetic events leading to aberrant activation of the MAPK pathway. The most common alterations are *KIAA1549:BRAF* fusions, $BRAF^{V600E}$ and *NF1* mutations. Novel drugs targeting the MAPK pathway (MAPKi) are prime candidates for the treatment of these single-pathway diseases. We aimed to develop an assay suitable for pre-clinical testing of MAPKi in pLGGs with the goal to identify novel MAPK pathway suppressing synergistic drug combinations.

A reporter plasmid (pDIPZ) with a MAPK-responsive ELK-1-binding element driving the expression of destabilized firefly luciferase was generated and packaged using a lentiviral vector system. Pediatric glioma cell lines with a BRAF fusion (DKFZ-BT66) and a $BRAF^{V600E}$ mutation (BT-40) background, respectively, were stably transfected. Modulation of the MAPK pathway activity by MAPKi was measured using the luciferase reporter and validated by detection of phosphorylated protein levels. A screen of a MAPKi library was performed and synergy of selected combinations was calculated.

Screening of a MAPKi library revealed MEK inhibitors as the class inhibiting the pathway with the lowest IC50s, followed by ERK and next-generation RAF inhibitors. Combination treatments with different MAPKi classes showed synergistic effects in BRAF fusion as well as $BRAF^{V600E}$ mutation backgrounds.

We here report a novel reporter assay for medium- to high-throughput pre-clinical drug testing in pLGG cell lines. The assay confirmed MEK, ERK and next-generation RAF inhibitors as potential treatment approaches for *KIAA1549:BRAF* and $BRAF^{V600E}$ mutated pLGGs. In addition, the assay revealed that combination treatments synergistically suppressed MAPK pathway activity.

Word count: 250/250

Introduction

Pediatric low-grade gliomas (pLGGs) are the most common brain tumors in children [1] and comprise various WHO grade I-II entities, including pilocytic astrocytomas (PAs) [2]. Complete surgical resection is the therapy of choice, but in case of unresectable tumors, chemo- or radiotherapy is applied (e.g. SIOP LGG 2004 trial, NCT00276640). The overall survival is good, with a 10-year survival rate of more than 90% [3, 4]. However, recurrences occur frequently, leading to a poor 10-year event free survival rate of only around 45% in this population [5]. The clinical course can be variable, requiring repeated periods of treatment. This often leads to chronic morbidity of the affected patients with significant neurological sequelae [6, 7]. Therefore, in spite of a good overall survival, the management of pLGGs requires novel therapeutic approaches to tackle disease- and therapy-related morbidity.

PA is a single-pathway disease with virtually all driving aberrations occurring in the RAS/ERK MAPK pathway. Recent studies in PAs have shown that around 70% of the underlying MAPK alterations are *KIAA1549:BRAF* fusions, followed by NF1 (7%), $BRAF^{V600E}$ (5%) and *FGFR1* (5%) mutations as the most frequent alterations [8]. Other mutations affecting MAPK pathway members such as *NTRK2, RAS* and *RAF1* are usually rare [8-10]. The majority (> 80%) of pLGGs other than PA also exhibit MAPK pathway activation [9]. While the BRAF fusion is typical for PAs, $BRAF^{V600E}$ mutations are frequently observed in pleomorphic xanthoastrocytomas (66%) and gangliogliomas (18%) [11]. Since most pLGGs and all PAs are driven by activation of a single pathway, targeting this axis is a promising treatment approach. Indeed, several small molecule MAPK inhibitors are currently under evaluation in clinical trials for pLGGs. The MEK inhibitor (MEKi) selumetinib has shown promising efficacy in pediatric patients with recurrent or refractory pLGG [12]. The MEKi trametinib is studied in patients with NF1 and recurrent or refractory pLGG (and/or plexiform neurofibroma) [13-15] or sporadic BRAF fusion positive pLGG in a phase I/II trial (NCT03363217). Treatment of pediatric patients with a $BRAF^{V600E}$ mutated pLGG with the combination of dabrafenib (V600E-specific BRAFi) and trametinib (MEKi) is currently being investigated in a phase I/II trial (NCT02684058). The novel RAF-inhibitor TAK-580 is in phase I clinical development in children with LGG and other MAPK driven tumors (NCT03429803). The upcoming LOGGIC Europe trial (EudraCT No. 2018-000636-10) will randomize patients with pLGG in a MEKi (trametinib) treatment arm and compare to standard of care (SOC) carboplatin/vincristine and to vinblastine monotherapy, respectively. Similarly, the upcoming COG trial ACNS1831 (NCT03871257) will randomize NF1 patients with pLGG to receive selumetinib or SOC carboplatin/vincristine. Finally, new pan-RAF and ERK inhibitors in (pre-)clinical development are potential candidates for treatment of BRAF fusion positive pLGGs [16-18].

Results of early clinical trials, however, emphasize the importance of fully understanding the underlying biology of MAPK signaling in pLGGs. 82% (9/11) of patients with recurrent or progressive pLGG treated with sorafenib, a multikinase inhibitor including BRAF in its inhibitory spectrum, showed progressive disease under treatment in a phase I/II study leading to early termination of the study [19]. Retrospectively it was shown that sorafenib indeed induced paradoxical activation of the MAPK pathway [20, 21]. These studies highlight the need for profound pre-clinical testing in suitable pLGG models and characterization of the mechanism of action of novel inhibitors before entering clinical trials.

To date, the availability of *in vitro* and *in vivo* models of pLGGs for pre-clinical drug testing is limited as pLGG cells typically undergo senescence *in vitro* and do not from tumors *in vivo*. We have established the first patient-derived *KIAA1549:BRAF* fusion expressing PA cell line, DKFZ-BT66 [22]. The model was shown to reflect the true biology of a PA including activation of the MAPK pathway, slow growth behavior resulting from oncogene-induced senescence (OIS) and positivity for the senescence-associated secretory phenotype (SASP), as well as responsiveness to MAPKi [22, 23]. However, the SV40 large T antigen expressed in DKFZ-BT66 cells, necessary to overcome OIS, limits the use of this cell line, as essential pro-apoptotic pathways are blocked [22, 24]. Direct measurement of MAPK pathway activity circumvents this problem when testing MAPKi in the DKFZ-BT66 model, in addition to providing biological information by direct measurement of actual pathway activity rather than a surrogate measure such as viability. In this study we have generated a novel ELK-1-driven luciferase reporter construct (pDIPZ) and applied it using a MAPKi compound library in both a BRAF fusion and a $BRAF^{V600E}$ mutated pLGG background in a medium- to high-throughput manner.

MATERIALS AND METHODS

Cell culture and cell lines

The patient-derived *KIAA1549:BRAF* fusion positive PA cell line DKFZ-BT66 is described in [22], the patient-derived $BRAF^{V600E}$ mutation positive pediatric glioma cell line BT-40 in [25]. The identity of all cell lines used was confirmed by Multiplex Cell Line Authentication (MCA) service and proven to be free of contamination by Multiplex cell Contamination Test (McCT) (http://www.multiplexion.de) [26, 27]. After testing for identity and contamination, cells were aliquoted and frozen in liquid nitrogen until further use. To establish the readout conditions of the assay, DKFZ-BT66 cells stably transduced with human telomere reverse transcriptase (hTERT) were used (described in [22]), however, for the drug screen and following combination treatments DKFZ-BT66 cells without overexpression of TERT were used. DKFZ-BT66 (+/-hTERT) cells (passage 9-14 for the native cell line and passage 18-30 for the hTERT cell line) were cultured in the presence of doxycycline (1µg/ml) to induce proliferation and BT-40 cells (passage 12-20) were cultured as described in [22]. Cell lines were tested for mycoplasma contamination with Venor®GeM Classic (cat. no. 11-1250, Minerva biolabs, Berlin, Germany) every four weeks. HEK293T cells (Brummer laboratory stock) were cultivated in DMEM (4.5 g/l glucose, 10% fetal calf serum (heat inactivated), 2 mM L-glutamine, 10mM HEPES, 200U/ml penicillin, 200µg/ml streptomycin) and transiently transfected as described previously in [28].

Plasmids

The vectors pDIPZ-ELK-1 binding site (BS)-CMVmin-desGFP-desFLuc (pDIPZ-CMV), pDIPZ-CMVmin-desGFP-desFLuc (pDIPZ-CMV w/o BS), pDIPZ-ELK-1 binding site-pFOSmin -desGFP-desFLuc (pDIPZ-pFOS) and pDIPZ-pFOSmin-desGFP-desFLuc (pDIPZ-pFOS w/o BS) were generated by modifying the pTRIPZ vector (cat. no. RHS4697, Dharmacon, Lafayette, Colorado, USA). For enzymatic digestion and ligation, the Anza Restriction Enzyme Cloning System (cat. no. IVGN3006, Thermo Fisher Scientific, Waltham, MA, USA) was used according to manufacturer's instructions. All primers were customized and purchased from Sigma-Aldrich (St. Louis, Missouri, USA). Primer sequences are listed in Suppl. Table S1. In summary, the gene cassette of the pTRIPZ vector, consisting of a doxycycline inducible promoter, a turboRFP cDNA and the shRNAmir cassette, was eliminated by digestion with Anza NotI (cat. no. IVGN001-4, Thermo Fisher Scientific) and Anza XbaI (cat. no. IVGN012-6, Thermo Fisher Scientific) and replaced by a reporter gene cassette. The reporter gene cassettes were kindly provided by Sebastian Herzog (*BIOSS*, Freiburg, Germany) used in two variations: one vector containing an ELK-1 binding site (serum response element [29]) linked to a CMVmin promoter (used for pDIPZ-CMV)

controlling the expression of destabilized GFP (desGFP) and destabilized firefly luciferase (desFLuc), and the other one harboring a pFOSmin promoter instead of CMVmin (used for pDIPZ-pFOS). These sequences were extracted by PCR (Q5® High-Fidelity DNA Polymerase, cat. no. M0491S, NEB, Ipswich, Massachusetts, USA) using primers with *NotI* and *XbaI* overhangs (Suppl. Table S1). After digestion with the respective enzymes, the sequence of interest was inserted into the pTRIPZ backbone. To allow selection in the puromycin-resistant DKFZ-BT66 cells [22], the puromycin resistance gene was replaced by a blasticidin resistance gene. The blasticidin resistance gene was extracted from the pDEST vector by PCR and then ligated into the altered pTRIPZ vector using the NEBuilder® HiFi DNA Assembly Cloning Kit (cat. no. E5520S, NEB) following manufacturer's instructions resulting in the generation of pDIPZ-CMV and pDIPZ-pFOS, respectively. Finally, to generate pDIPZ-CMV w/o BS and pDIPZ-pFOS w/o BS, the ELK-1 binding site was eliminated by PCR amplification of the whole plasmid while excluding the binding site.

The cDNA for HA-tagged $BRAF^{WT}$ was amplified from pBabe-puro/$BRAF^{WT}$-HA [10] using the oligonucleotides NotIBRAFfwd and BRAF C-term-HA (Suppl. Table S1). Both primers introduce flanking NotI sites into the amplicon, which was subcloned into pSC-A (Stratagene) for further propagation. The cDNA was then recovered by NotI digestion and subcloned into NotI linearized pMIBerry-NotI unique [30] to yield pMIBerry NotI unique/BRAFWT-HA. This retroviral vector allows for the expression of a bicistronic transcript encoding the protein-of-interest and dsRed2. The V600E mutation was introduced into this plasmid using site-directed mutagenesis standard procedures and the primers hBRAFV600Efwd and hBRAFV600Erev (Suppl. Table S1). For the generation of pMIBerry NotI unique/KIAA1549:BRAF-HA, the cDNA for long-form KIAA1549:BRAF (KEx16BEx9) fusion was amplified from pBABE-puro/KIAA1549-BRAF [10] using the primers MfeIKIAA1549fwdI and MfeIKIAA1549rev (Suppl. Table S1). The amplicon was subcloned into pSC-A for propagation, recovered by MfeI digestion and subcloned into pMIBerry-NotI unique. The BRAF cDNAs of all pMIBerry-NotI unique constructs were confirmed by DNA sequencing.

Lentiviral transduction

Lentiviral packaging and transduction were performed as described in [22]. For antibiotic selection of DKFZ-BT66 (hTERT) and BT-40 cells, blasticidin (cat. no. A1113903, Thermo Fisher Scientific) was used in a final concentration of 6µg/ml (for the hTERT cell line 10µg/ml) and 2µg/ml, respectively, for ten days.

MAPK inhibitors and other drugs

A MAPK inhibitor library (cat. no. L3400) and chemotherapeutics (carboplatin: cat. no. S1215, vinblastine: cat. no. S1248 and vincristine: cat. no. S1241) were purchased from

Selleckchem (Houston, Texas, USA). This pre-dissolved set of drugs was stored at -80°C until usage. Additionally, the following investigational MAPK inhibitors were added to the library: LXH254 (structure available here: [31]) and LTT462 (both generously provided by Novartis, Cambridge MA, USA), RAF709 (cat. no. 23820, Cayman Chemical, Ann Arbor, Michigan, USA), PLX7904 (cat. no. S7964, Selleckchem), PLX8394 (cat. no. HY-18972, MedChemExpress, Monmouth Junction, New Jersey, USA), LY3009120 (cat. no. S7842, Selleckchem), LY3214996 (structure available here: [32]) (generously provided by Eli Lilly and Company, Indianapolis, Indiana, USA), (5Z)-7-oxo zeaenol (cat. no. 17459, Cayman Chemical), SCH772984 (cat. no. 19166, Cayman Chemical) and BI-882370 (cat. no. 24273, Cayman Chemical). These drugs were dissolved in DMSO, aliquoted and stored at -80°C until usage. Inhibitors were diluted in cell culture medium and added to the cell culture at the indicated concentrations for the indicated time.

Metabolic activity

Measurement of metabolic activity was conducted in white flat bottom 384-well plates (cat. no. 3570, Corning, New York, USA) 72 hours after drug treatment, using a CellTiter-Glo® One Solution assay (cat. no. G8461, Promega, Madison, WI, USA) following manufacturer's instructions. Cells were seeded one day before treatment with n=3 x 10^3 DKFZ-BT66 cells per well and n=6 x 10^3 BT-40 cells per well in 384-well plates. After drug treatment for 72 hours with concentrations ranging from 0.0043 to 25000 nM, metabolic activity was measured by Multimode Microplate Reader (Tecan). The metabolic activity screen was done in a single run with single measurements of each drug concentration step.

Luciferase reporter assay

Measurement of luciferase activity was conducted in white flat bottom 96- or 384-well plates (cat. no. 781094, 781096, Greiner Bio-One, Kremsmünster, Austria) after 24 hours of treatment using a Luciferase Assay System (cat. no. E1500, Promega, Madison, Wisconsin, USA). For experiments conducted in 96-well plates, 25 µl of luciferase substrate were added to each well. Steady-Glo® Luciferase Assay System (cat. no. E2510, Promega) was used for experiments conducted in 384-well plates following manufacturer's instructions. DKFZ-BT66 pDIPZ cells were seeded 24 hours prior to treatment in the presence of 1µg/ml doxycycline with n=5 x 10^4 cells per well in 96-well plates and n=1 x 10^4 cells per well in 384-well plates. BT-40 pDIPZ cells were seeded 24 hours before treatment with n=1 x 10^5 cells per well in 96-well plates and n=2 x 10^4 cells per well in 384-well plates. After drug treatment for 24 hours, luciferase activity was measured using the FLUOstar OPTIMA automated plate reader (BMG Labtech). For the MAPKi screen, cells were treated in nine concentration steps ranging from 0.001 nM to 10000 nM. IC50 values obtained from the screen ($IC50_{screen}$) were

validated ($IC50_{validated}$) in three independent replicates (Suppl. Table S5). In the combination experiments, cells were treated with nine concentration steps in a serial dilution with each individual $IC50_{validated}$ as the middle concentration. All experiments (except the MAPKi reporter screen) were conducted in three biological replicates. The reporter screen was done in a single run with three technical replicates for each drug concentration step.

Western blot

Western blots were performed as described previously [33]. The following antibodies were used: Monoclonal rabbit pERK (1/2) (Thr202/Tyr204) (1:500, cat. no. 4377, Cell Signaling Technology, Danvers, Massachusetts, USA), monoclonal rabbit total ERK (1/2) (1:1000, cat. no. 4695, Cell Signaling Technology), monoclonal rabbit anti-RSK1 p90 phospho T359 and S363 (1:1000, cat. no. ab32413, Abcam, Cambridge, United Kingdom), monoclonal rabbit RSK1 p90 (1:500, cat. no. 9333S, Cell Signaling Technology), monoclonal rabbit phospho-MEK1/2 (1:1000, cat. no. 9121S, Cell Signaling Technology), monoclonal rabbit MEK1/2 (1:1000, cat. no. 9122S, Cell Signaling Technology), monoclonal mouse HA-Tag (1:2000, cat. no. 9110, Abcam), monoclonal rabbit BRAF C-19 (1:750, cat. no. sc-166, Santa Cruz Biotechnology, Santa Cruz, California, USA) and monoclonal mouse GAPDH (1:10000, cat. no. MAB374, Merck, Darmstadt, Germany). Cells were treated with the indicated drugs in the indicated concentrations for 24 hours. Depicted blots are representative of at least three biological replicates. Quantification of Western blot bands was conducted using ImageJ on Windows.

Flow cytometry

Measurement of GFP was conducted using a Merck Guava EasyCyte HT flow cytometer. GFP and RFP were measured using a 488 nm laser (500 long pass filter, 512/18 band pass filter) and a 561 nm laser (593 long pass filter, 620/52 band pass filter), respectively. Data was analyzed using FlowJo-V10 software and GuavaSoft version 3.1.1 (Merck Millipore).

For the assessment of GFP positive cells (Fig. 1) DKFZ-BT66 or BT-40 cells +/- pDIPZ constructs were seeded in 6-well plates (n=1.5 x 10^5/well) 24 hours prior to measurement. After 24 hours, cells were prepared for flow cytometry by short enzymatic digestion with 0.05% trypsin-EDTA (cat. no. 25300054, Thermo Fisher Scientific) and subsequent addition of cold PBS plus 2% FBS (cat. no. F7524, Sigma-Aldrich). Depicted blots are representative of three technical replicates (Fig. 1). For evaluation of fluorescence under MAPKi treatment (Fig. 2A) DKFZ-BT66 pDIPZ cells (n=5 x10^4/well) or BT-40 pDIPZ cells (n=1 x10^5/well) were seeded in clear flat bottom 96-well plates (cat. no. 3072, Corning) 24 hours prior to treatment. After 24 hours of treatment, cells were prepared for flow cytometry as stated above. Depicted blots are representative of three biological replicates (Fig. 2A).

Drug combination analysis

Determination of the combination index (CI) and generation of isobolograms were conducted using the Chou-Talalay method and CompuSyn software on Windows for experiments using concentration ranges [34].

Synergism was further validated for selected RAFi/MEKi and RAFi/ERKi combinations using pERK or pRSK detection by Western blot as a readout. Concentrations were chosen according to the corresponding isobologram generated for the 0.9 fraction affected (Fa), i.e. $Drug1_{IC90}$, $Drug2_{IC90}$, $Drug1_{Combi}$+$Drug2_{Combi}$ leading to 90% inhibition of the pathway, $Drug1_{Combi}$, $Drug2_{Combi}$. Western blot signal was quantified and the effect of the combination of both drugs was compared to the effect of each individual components allowing the calculation of a CI value using the Bliss independence model as described in [35].

Statistics

All experiments were conducted in at least three biological triplicates, except the flow cytometry validation (Fig. 1) and the reporter screening of MAPK inhibitors (Fig. 3, Suppl. Table S3) which was conducted in a single run with three technical replicates and the metabolic activity screen, which was conducted in a single run without replicates. Significance was calculated using the Tukey's 'Honest Significant Difference' method in R on Windows [36, 37] and p-values <0.05 were considered significant. IC50 values were calculated using GraphPad Prism version 5.01 (GraphPad Software, La Jolla, California, USA) on Windows. Graphs and CI tables were generated using GraphPad Prism version 5.01, FlowJo-V10 software, Microsoft PowerPoint 2010, Microsoft Excel 2010 on Windows.

RESULTS

Metabolic activity readout is unsuitable to assess MAPKi treatment in SV40 large T expressing DKFZ-BT66 cells

To identify novel treatment options for pLGG an initial screen with different classes of MAPKi was performed. Metabolic activity was measured using an ATP-based assay in the *KIAA1549:BRAF* fusion positive pilocytic astrocytoma cell line DKFZ-BT66 and the $BRAF^{V600E}$ mutation positive pediatric glioma cell line BT-40 after treatment with various MAPKi for 72h (Suppl. Fig. S1). However, most MAPKi and other drugs including chemotherapy failed to reduce metabolic activity at clinically relevant concentrations in DKFZ-BT66 cells. This is most likely due to the fact that pro-apoptotic pathways are blocked by the SV40 large T antigen (present in DKFZ-BT66 but not in BT-40), as described in [22]. Only compounds not dependent on e.g. p53 for induction of cell growth arrest, such as vincristine and vinblastine, showed an effect at clinically relevant concentrations in DKFZ-BT66 (Suppl. Fig. S1). In contrast, BT-40, which does not express SV40 large T antigen, showed reduced metabolic activity after MAPKi treatment (Suppl. Fig. S1). We thus concluded that metabolic activity is not suitable as a readout for a drug screen in the *KIAA1549:BRAF* fusion positive model DKFZ-BT66.

Generation of the novel ELK-1 reporter construct pDIPZ and transduction into two patient-derived pediatric glioma models

In order to enable medium- to high-throughput screening of MAPKi in a *KIAA1549:BRAF* fusion (in addition to a $BRAF^{V600E}$ mutant) background we aimed at direct assessment of MAPK pathway activity instead of metabolic activity. We generated an ELK-1 responsive lentiviral reporter plasmid to directly measure MAPK pathway activity [29] and introduced it into both cell models. Destabilized GFP (desGFP) and destabilized firefly luciferase (desFLuc), separated by a T2A site and controlled by either a CMVmin or a pFOSmin promoter region (pDIPZ-CMV or -pFOS), were used as reporter genes (Fig. 1A; I and III). The promoter region was linked to an ELK-1 binding element, modulating the expression of the reporter genes depending on MAPK pathway activity [29]. In addition, we generated both plasmids without the ELK-1 responsive element (pDIPZ-CMV/pFOS w/o binding site) as controls (Fig. 1A; II and IV). Lentiviral transduction efficiency was assessed by flow cytometry: ~56% and ~49% of DKFZ-BT66 hTERT cells (Fig. 1B), and ~37% and ~40% of BT-40 cells (Fig. 1C) transduced with pDIPZ-CMV and pDIPZ-pFOS, respectively, were assessed as GFP positive.

Characterization of reporter signal and promoter response

In order to evaluate the signal range of the different reporter genes and promoters, the highly selective MEK inhibitor (MEKi) trametinib and the $BRAF^{V600E}$ inhibitor (BRAFV600Ei) vemurafenib were tested in both genetic backgrounds, *KIAA1549:BRAF* fusion (DKFZ-BT66 hTERT pDIPZ) and $BRAF^{V600E}$ mutation (BT-40 pDIPZ). A strong and significant decrease of the luminescence signal under MEKi treatment was detected in both the *KIAA1549:BRAF* fusion as well as the $BRAF^{V600E}$ mutation background (Fig. 2A). The luminescence signal decreased after trametinib (MEKi) treatment by 65-67% in the *KIAA1549:BRAF* fusion background (CMV: 67.1% +/- 3.6%; pFOS: 64.6% +/- 9.4%; % reduction in luminescence of untreated control) and by 72-74% in the $BRAF^{V600E}$ mutation background (CMV: 71.7% +/- 7.2%; pFOS: 74.4% +/- 1.7%; % reduction in luminescence of untreated control) (Fig. 2A). The luminescence signal after vemurafenib (BRAFV600Ei) treatment decreased in a differential manner, as expected. The luminescence signal decreased by 59-63% in the $BRAF^{V600E}$ mutation background (CMV: 58.6% +/- 5.9%; pFOS: 63.0% +/- 7%; % reduction compared with untreated control), while no decrease in signal was observed in the *KIAA1549:BRAF* fusion background (Fig. 2A). In contrast, the decrease in fluorescence signal determined by flow cytometry was not significant in the *KIAA1549:BRAF* fusion background, and only limited in the $BRAF^{V600E}$ mutation background (Fig. 2A) with a reduction of only e.g. 16-32% as determined by flow cytometry (after trametinib treatment: CMV: 32.1% +/- 5.8%; pFOS: 22.6% +/-6.1%; after vemurafenib treatment: CMV: 27.2% +/- 4.0%; pFOS: 16.3% +/- 2.8%; % reduction compared with untreated control) (Fig. 2A). In conclusion, a significant reduction in luminescence, but not in fluorescence, in a mutational background specific manner, was detectable in both cell lines. This is possibly due to prolonged protein stability of desGFP leading to slow response dynamics. We therefore chose luminescence as the reporter signal in the following experiments.

The two reporter plasmids with different promoters, pDIPZ-CMV and pDIPZ-pFOS, were compared by measurement of luminescence after treatment with trametinib (MEKi) for 24h in the *KIAA1549:BRAF* fusion and the $BRAF^{V600E}$ mutation background. No significant difference between the two promoters was observed (Fig. 2B). Calculated relative IC50 values as well as dose-response curve shapes were similar, indicating that both promoters perform equally well in the setting of this assay. Since no difference in signal output was detectable between both promoters, we arbitrarily chose the pDIPZ-CMV reporter plasmid for all subsequent measurements.

In order to control for unspecific changes in desFLuc expression upon MAPKi treatment we measured luminescence using a pDIPZ-CMV reporter plasmid without the ELK-1 binding site (pDIPZ-CMV w/o ELK-1 binding site) and compared it to the pDIPZ-CMV reporter plasmid

with the ELK-1 binding site (pDIPZ-CMV w/ ELK-1 binding site). Importantly, modulation of MAPK pathway activity by trametinib treatment in both *KIAA1549:BRAF* fusion and $BRAF^{V600E}$ mutation background did not result in signal suppression when using the pDIPZ-CMV w/o ELK-1 binding site (Fig. 2C). Therefore, we conclude that the ELK-1 binding site is specific for mediating MAPK pathway activity to the reporter plasmid.

Finally, the results of the reporter assay were validated by Western blot analysis. As expected, a concentration dependent decrease in phosphorylation of ERK was seen in accordance with the loss of MAPK dependent signal measured by the luminescence reporter pDIPZ-CMV (Fig. 2D). Further measurements using the luminescence assay were normalized to treatment with trametinib (1µM), since the MAPK pathway was maximally suppressed under this condition (Fig. 2B and 2D). In summary, the changes in reporter signal upon MAPKi treatment are indeed reflective of changes in MAPK pathway activity, and therefore the pDIPZ-CMV reporter is suitable for a MAPKi drug screen.

Screening of a MAPKi drug library reveals ERK inhibitors as a novel potent class beyond MEK and RAF inhibitors inhibiting the MAPK pathway in low-grade gliomas

In order to evaluate the effects of different inhibitors on MAPK pathway activity, we used our reporter assay to screen a commercially available MAPKi library customized to contain additional RAF, MEK and ERK inhibitors (see Suppl. Table S2). MEKi was the dominant drug class inhibiting the pathway at very low IC50 levels as determined in the screen ($IC50_{screen}$) in both the *KIAA1549:BRAF* fusion as well as the $BRAF^{V600E}$ mutation background. Trametinib, a dual mechanism MEK inhibitor [38], was the top hit in both backgrounds (Fig. 3A, B and C). Of note, MEKi, e.g. trametinib, pimasertib or selumetinib, also paradoxically activated the MAPK pathway at lower concentrations in the $BRAF^{V600E}$ mutation background (BT-40 cells) (Fig. 3B). All ERKi included in the library (SCH772984, ulixertinib, GDC-0994, LY3214996, LTT462, (5Z)-7-oxo zeaenol) also showed potent inhibition of the MAPK pathway in both cell lines, with $IC50_{screen}$ values below 130nM.

As expected, strong differences in pathway inhibition were observed for RAFi between the *KIAA1549:BRAF* fusion and the $BRAF^{V600E}$ mutation background (Fig. 3C). Most RAFi, especially first and second generation RAFi, such as vemurafenib [17] paradoxically activated the pathway in the *KIAA1549:BRAF* fusion background (DKFZ-BT66) (Fig. 3A), as has been described previously [20, 21, 39]. Of note, the so-called paradox breakers [40] PLX7904 (PLX PB-4) [41] and its optimized analogue PLX8394 (PLX PB-3) [21] did not show reduction of pathway activity in the *KIAA1549:BRAF* fusion background (Fig. 3A). This is in contrast to reports on PLX7904 impairing ERK phosphorylation in *NRAS* mutant

vemurafenib-resistant melanoma cells [41], and PLX8394, which was described to fully abrogate the MAPK pathway in *KIAA1549:BRAF* fusion expressing cell lines [21]. There were, however, some newly developed third generation pan-RAFi, e.g. LY3009120 or LXH254 [17, 42, 43], which successfully inhibited the pathway - with $IC50_{screen}$ values ranging from 270nM to 830nM in the *KIAA1549:BRAF* fusion background (Fig. 3A). Furthermore both AZ628, a pan-RAF inhibitor which has a high potency against CRAF [44], and RAF709, a selective inhibitor of dimeric RAF and monomeric mutant BRAF [45], were able to inhibit the MAPK pathway in the *KIAA1549:BRAF* fusion background (DKFZ-BT66) at higher concentration ranges. In the $BRAF^{V600E}$ mutation background (BT-40) almost all RAFi were effective, with $BRAF^{V600E}$-specific inhibitors like dabrafenib or encorafenib scoring as top hits (Fig. 3B).

Overall, $IC50_{screen}$ estimated for RAF and ERK inhibitors were significantly lower in the $BRAF^{V600E}$ expressing cell line than the BRAF fusion model (Fig. 3C). Other drugs such as JNK-, p38α-inhibitors or chemotherapeutics showed no inhibitory effect on measured MAPK pathway activity in either the *KIAA1549:BRAF* fusion or the $BRAF^{V600E}$ mutation background, and thus $IC50_{screen}$ values could not be estimated.

To ensure that the decrease in luminesce signal under treatment resulted from MAPK pathway inhibition and is thus ELK-1 dependent [29], cells transduced with the control vector pDIPZ w/o ELK-1 binding site were treated with the $IC50_{screen}$ concentrations of each drug and luminescence was subsequently measured. Only TAK-632, carboplatin, sorafenib and sorafenib tosylate, or sorafenib tosylate and PLX-4720, showed a signal reduction below 80% in DKFZ-BT66 or BT-40, respectively, indicating that these could be false positive hits in the screen (Suppl. Table S3).

To validate key findings in the screen, pERK protein levels after treatment with selected inhibitors were determined by Western blot. The difference in response to vemurafenib treatment is shown in Fig. 4A. Paradoxical activation was observed for DKFZ-BT66, whereas pERK signal was reduced in BT-40, similar to the results obtained from the screen (Fig. 3A and B). In contrast to vemurafenib, the second generation RAFi AZ628 was able to reduce pERK levels in the *KIAA1549:BRAF* fusion background as seen in Fig 4B further validating the reporter assay being suitable to distinguish between positive and negative hits.

Finally, the differential response to the so-called paradox breakers in both backgrounds was validated by assessment of pERK levels (Fig 4C). Treatment with the 3rd generation RAFi PLX8394, the optimized analogue of PLX7904 [40], significantly reduced pERK levels in the $BRAF^{V600E}$ background in low concentrations (1nM) (Fig. 4C), as expected from the reporter assay data. In contrast, pERK levels were significantly reduced only at very high

concentrations in the BRAF fusion background, in accordance with the signal observed in the reporter assay (Fig. 3A). Importantly, paradoxical activation on pERK level was not observed in the BRAF fusion background.

To validate our findings in additional genetic models and to evaluate if this observation is independent of the genetic backgrounds of the cells, HEK293T cells overexpressing different MAPK pathway alterations were treated with PLX8394 (Fig. 4D and E). The overexpression of $BRAF^{V600E}$ protein was validated by detection of the HA-tag and of the *KIAA1549:BRAF* protein by detection of the fusion-length BRAF protein (Suppl. Fig. 2). Reduction of pMEK (as direct readout of RAF inhibition) and pERK (as direct readout of MEK inhibition) levels were achieved under lower concentrations of PLX8394 for $BRAF^{V600E}$ mutation compared to *KIAA1549:BRAF* fusion expressing HEK293T cells (Fig. 4D and E). In conclusion, the $BRAF^{V600E}$ mutated background is more susceptible to the treatment with the paradox breaker PLX8394, as predicted by the reporter assay (Fig. 3A and B).

In summary, MEKi and ERKi effectively inhibited MAPK pathway activity in both the *KIAA1549:BRAF* fusion as well as the $BRAF^{V600E}$ mutation background, as measured by the reduction in luminescence signal. In case of RAFi, pathway inhibition depended on the type of MAPK aberration and RAFi class, as expected. Other drugs tested, apart from MEKi, ERKi, and RAFi, were not able to reduce the MAPK pathway signal output.

Combination of different classes of MAPKi show synergistic effects on pathway inhibition in the *KIAA1549:BRAF* fusion as well as the $BRAF^{V600E}$ mutation background

To further assess novel potential treatment regimens for pLGG we tested combinations of different classes of MAPKi for synergistic inhibition of the MAPK pathway. Combinations of different MAPKi were chosen on the basis of lowest $IC50_{screen}$ values for each respective background, as well as matching compounds from a single pharmaceutical company in a pragmatic approach to model possible future clinical trials (Suppl. Table S4). $IC50_{screen}$ values generated in the screen of the drugs chosen for combination testing were validated ($IC50_{validated}$) (Suppl. Table S5). $IC50_{validated}$ were used for the combination experiments. Synergistic effects were observed in all tested RAFi and MEKi combinations in both *KIAA1549:BRAF* fusion (LXH254 plus trametinib and AZ628 plus selumetinib) as well as the $BRAF^{V600E}$ mutation background (AZ628 plus selumetinib, vemurafenib plus cobimetinib and dabrafenib plus trametinib) (Fig. 5A; Suppl. Fig. S3-S5). All synergies measured by combination index (CI) plotting were corroborated by isobologram analysis (Suppl. Fig. S5).

Synergy of the combination of RAFi and ERKi was detected only for one of the ERKis tested. Only the ERKi LTT462 showed synergy in combination with the RAFi LXH254 in the *KIAA1549:BRAF* fusion and with dabrafenib in the $BRAF^{V600E}$ mutation background, respectively (Fig. 5A; Suppl. Fig. S3-S5). All other RAFi plus ERKi combinations (LY3009120 plus LY3214996, dabrafenib plus ulixertinib, encorafenib plus ulixertinib, encorafenib plus GDC-0994), as well as MEKi plus ERKi combinations (trametinib plus LTT462, pimasertib plus SCH772984) revealed only additive or even antagonistic effects, however mostly in the form of buffering-antagonism [46] (Fig. 5A).

To validate the synergistic effects observed for the combination of RAFi and MEKi, and RAFi and ERKi, respectively, Western blots were conducted and synergistic effects were calculated using the Bliss independence model [35] (Fig. 6). For the RAFi AZ628 in combination with the MEKi selumetinib synergistic effects were observed in both cell lines using pERK as readout (Fig. 6A and B) with CI values below 0.9. For the combination of the RAFis (LXH254 and dabrafenib, respectively) with the ERKi (LTT462) pRSK levels as a downstream target of pERK were determined to evaluate synergism, since pERK cannot be used as readout due to accumulation of pERK upon inhibition with the ERKi (as described previously [47]), especially in the *KIAA1549:BRAF* fusion background (Fig. 6A). For both backgrounds CI values around 1.0 were calculated from the protein quantification by Western blot, indicating additive effects (Fig. 6A and B).

In summary (Fig. 5B), synergistic effects were observed for treatment with RAFi and MEKi and some of the RAFi and ERKi combinations in both the *KIAA1549:BRAF* fusion as well as the $BRAF^{V600E}$ mutation background. The combination of MEKi and ERKi did not reveal unequivocal synergism but rather additive and/or antagonistic (if buffered) effects.

Discussion

pLGGs are a chronic condition often associated with multiple recurrences and therapeutic interventions in the course of a patient's lifetime, and new effective drug treatments are urgently needed. Despite several ongoing early clinical trials testing MAPKi (alone and in combination) in pLGGs (e.g. NCT02285439; NCT01089101; NCT03363217; NCT02684058), extensive pre-clinical studies analyzing the efficacy of MAPKi in pLGGs are still missing. The most important reason for this is the lack of suitable pLGG models that faithfully reflect the biological features of these tumors, including genetic background, slow growth, and induction of senescence. The strength of our study is the use of patient-derived pLGG models and a fast and cost-effective reporter system suitable for high-throughput analysis.

Previous studies have established several *in vitro* and *in vivo* pLGG models (e.g. [10, 21, 48-50]), most of them genetically engineered to overexpress the most common BRAF aberrations. However, the underlying MAPK driver mutation, specifically the *KIAA1549:BRAF* fusion, is not expressed endogenously in these models. The expression levels and relative stoichiometry of BRAF, CRAF and the BRAF fusion are altered, and therefore interactions and feedback mechanisms within the MAPK pathway are likely to be artificially changed. In our study we have used two well-characterized patient-derived pediatric glioma cell lines endogenously expressing the *KIAA1549:BRAF* fusion or the $BRAF^{V600E}$ mutation without genetic overexpression [22, 25].

Widely used methods to determine MAPK pathway activity are e.g. Western blot for pERK, qPCR for MAPK pathway genes, and serum response element (SRE) luciferase reporter assays based on transient transfection [51, 52]. These methods are not well suited for high-throughput analysis of the MAPK pathway due to workload, time, and scalability reasons. Here we use a reporter assay which comes with several advantages: stable lentiviral transduction, no individual sample processing after treatment, fast measurement, scalability and automatability of the cost-effective readout. In addition, the ELK-1-responsive design of the reporter assay provides information on the transcriptional sum output of the MAPK pathway instead of measurement of phosphorylation status of single components of the pathway, such as pERK, alone. The importance of this information is emphasized by past studies, e.g. showing that in tumors with mutations in BRAF or receptor tyrosine kinase (RTK), although having similar levels of pERK, elevated transcriptional output of the MAPK pathway was detected only in BRAF mutated tumors [53]. Consequently, only BRAF mutated tumors were dependent on ERK signaling for proliferation and MEKi sensitive [53]. The reporter assay described here can not only measure the actual transcriptional output of the MAPK pathway, but also compare relative changes upon treatment with MAPKi. This allows for comparison of relative potencies of MAPKi in pLGG.

The pattern of effectiveness in MAPK inhibition both on the single compound as well as the MAPKi class level warrants a closer look at the molecular effectors of MAPK inhibition. Most of the early generation RAF inhibitors led to paradoxical activation as expected, and not all pan-RAFi could inhibit the MAPK pathway. Conversely, novel third generation pan-RAFi showed inhibitory activity with minimal paradoxical activation in the $BRAF^{V600E}$ background as well as in the *KIAA1549:BRAF* fusion positive cell line. Strikingly, all of the RAF inhibitors capable of inhibiting the pathway in the BRAF fusion expressing cell line belong to type II inhibitors, which stabilize the αC-helix in the IN and the DFG motif in the OUT conformation [17, 54]. This mechanism prevents negative allosteric movements of the second protomer of the RAF dimer, which keeps its αC-helix IN conformation. As a result, the inhibitor is able to bind to the second RAF protomer in similar concentrations, to completely abolish kinase activity. Interestingly, the paradox breakers PLX7904 and PLX8394 were less effective in BRAF fusion containing cells compared to their $BRAF^{V600E}$ positive counterparts. Similarly, Weinberg *et al.* [30] observed that the paradox breakers PLX7904 and PLX8394 were more effective in suppressing MEK/ERK phosphorylation triggered by $BRAF^{V600E}$ than by the *TTYH3:BRAF* fusion protein. This might be explained by the fact that PLX7904 and PLX8394 were developed with vemurafenib as starting point [55]. Vemurafenib was optimized for the conformation of V600E that is stabilized by the mutation specific salt-bridge created by E600 [56]. The kinase domain of BRAF fusions, however, is not mutated and is therefore probably much more flexible, leading to less sensitivity to the paradox breakers. Alternatively, but not excluding this possibility, other mechanisms might contribute to the insensitivity of *KIAA1549:BRAF* to PLX8394. Recently, Botton *et al* also reported the insensitivity of various BRAF fusion driven melanoma lines towards PLX8394. They suggest that this paradox breaker, which was originally selected to impair the activity of RAS-induced BRAF/RAF1 heterodimers, fails to disrupt RAS-independent kinase homo-dimers of the BRAF kinase domains whose stability might be additionally influenced by their fusion partner [57]. In that regard, it should be noted that, despite its frequency as BRAF fusion partner, very little is known about the tertiary and quaternary structures of KIAA1549.

MEKi were the most effective class of MAPKi in both genetic backgrounds based on $IC50_{screen}$ reporter values. Specifically trametinib, a potent inhibitor of MEK1/2 which also reduces the activation of MEK by RAF by disrupting the conformation of the MEK1/2 activation loop sites (a so-called 'feedback buster') [38, 58], showed the lowest IC50s in both backgrounds. Furthermore, our data indicate that MEK inhibitors are acting in clinically achievable concentrations (Suppl. Fig. S3 and S4), suggesting a high potential of sufficient MAPK pathway suppression also in patients. ERKi were also an effective class of MAPKi in both backgrounds. Current clinical phase I studies (e.g. NCT02857270, NCT02711345,

NCT01875705) will show if these promising MAPKi will qualify as potential candidates for future pLGG trials [18].

The rationale behind combination treatments is based on the inhibition of potential escape mechanisms from therapy via feedback activation as well as the possibility to reduce individual drug concentrations, and thus drug toxicities, in combination settings. Reconstitution of ERK signaling as a resistance mechanism, e.g. via RAF dimer formation, has been observed in malignant transformation of pLGGs (although this is a rare event) [59]. Other resistance mechanisms described in e.g. melanoma [60] are BRAF amplification or MEK mutation, leading to resistance to MAPKi single treatment by reconstitution of MAPK pathway signaling. Combination treatments targeting several components of the pathway could effectively prevent tumor progression under such circumstances [61]. Synergistic effects of a pan-RAF/MEK inhibitor combination were confirmed for $BRAF^{V600E}$ inhibitor resistant melanoma and colorectal carcinoma cell lines [62]. In addition, the phase I clinical trial of vemurafenib in melanoma patients revealed that a complete shutdown of the MAPK pathway is necessary for significant tumor response [56] which could be more easily achieved using synergistic combination treatments. Our results suggest that strong synergy depends on the combination of certain classes of MAPKi. Synergistic effects were observed when RAFi were combined with either MEKi or ERKi, possibly due to directly targeting the BRAF alteration in both mutational backgrounds. In case of the combination of MEKi with ERKi, synergistic effects were virtually absent. This is consistent with a recently published study describing that MEKi and ERKi combinations act synergistically only in *RAS* mutant models but not in BRAF mutant models as a consequence of distinct feedback productivity [63].

Finally, the results obtained from the reporter assay could be validated by Western blot: synergistic effects were confirmed for RAFi combined with a MEKi. The combinations of RAFis and ERKi revealed rather additive effects instead of the synergism indicated by the reporter assay. The downstream target pRSK was chosen as a suitable readout for ERK inhibition since pERK is accumulating upon ERKi treatment. Indeed, a reduction of pRSK, indicative of ERK inhibition, was readily detectable. Considering the measurement of synergism by Western blot however, detection of rather small effects (such as phospho-protein changes) by Western blot can be challenging. Measuring the phosphorylation of a single protein such as RSK downstream of pERK as a readout could disregard its own feedback mechanisms interfering with a strong dynamic reaction. Our assay using a sensitive luminescence signal as a surrogate marker of transcriptional activity at the downstream end of the MAPK pathway might be more suitable to evaluate synergistic effects on the global signaling output.

In summary we have generated a novel MAPK-specific reporter assay in a pLGG-specific background. This reporter assay enables direct assessment of transcriptional activation status of the MAPK pathway and response to MAPKi treatment. Our results indicate that, in addition to MEKi, ERKi and next-generation pan-RAFi are novel potential candidates for the treatment of pLGGs. The synergy of the combination of RAFi with either MEKi or ERKi detected in both genetic backgrounds (*KIAA1549:BRAF* fusion and $BRAF^{V600E}$ mutation) indicates strong clinical potential of those MAPKi combinations. Clinical trials are urgently needed to test the efficacy of MAPKi combination therapies, especially RAFi and MEKi, in pLGGs.

633 **Acknowledgments**

634 We thank Daniela Kuhn, Isabel Büdenbender and Sandra Braun for excellent technical
635 assistance.

References

1. Ostrom, Q.T., H. Gittleman, P. Liao, T. Vecchione-Koval, Y. Wolinsky, C. Kruchko et al., *CBTRUS Statistical Report: Primary brain and other central nervous system tumors diagnosed in the United States in 2010-2014.* Neuro Oncol, 2017. **19**(suppl_5): p. v1-v88.

2. Louis, D.N., A. Perry, G. Reifenberger, A. von Deimling, D. Figarella-Branger, W.K. Cavenee et al., *The 2016 World Health Organization Classification of Tumors of the Central Nervous System: a summary.* 2016. **131**(6): p. 803-820.

3. Burkhard, C., P.L. Di Patre, D. Schuler, G. Schuler, M.G. Yasargil, Y. Yonekawa et al., *A population-based study of the incidence and survival rates in patients with pilocytic astrocytoma.* J Neurosurg, 2003. **98**(6): p. 1170-4.

4. Colin, C., L. Padovani, C. Chappe, S. Mercurio, D. Scavarda, A. Loundou et al., *Outcome analysis of childhood pilocytic astrocytomas: a retrospective study of 148 cases at a single institution.* Neuropathol Appl Neurobiol, 2013. **39**(6): p. 693-705.

5. Gnekow, A.K., F. Falkenstein, S. von Hornstein, I. Zwiener, S. Berkefeld, B. Bison et al., *Long-term follow-up of the multicenter, multidisciplinary treatment study HIT-LGG-1996 for low-grade glioma in children and adolescents of the German Speaking Society of Pediatric Oncology and Hematology.* Neuro-oncology, 2012. **14**(10): p. 1265-1284.

6. Zuzak, T.J., A. Poretti, B. Drexel, D. Zehnder, E. Boltshauser, and M.A.J.C.s.N.S. Grotzer, *Outcome of children with low-grade cerebellar astrocytoma: long-term complications and quality of life.* 2008. **24**(12): p. 1447.

7. Laroussinie, F., S. Puget, C. Sainte- Rose, and G. Dellatolas, *Long-term functional outcome of patients with cerebellar pilocytic astrocytoma surgically treated in childhood AU - Ait Khelifa-Gallois, N.* Brain Injury, 2015. **29**(3): p. 366-373.

8. Jones, D.T.W., B. Hutter, N. Jäger, A. Korshunov, M. Kool, H.-J. Warnatz et al., *Recurrent somatic alterations of FGFR1 and NTRK2 in pilocytic astrocytoma.* Nature genetics, 2013. **45**(8): p. 927-932.

9. Zhang, J., G. Wu, C.P. Miller, R.G. Tatevossian, J.D. Dalton, B. Tang et al., *Whole-genome sequencing identifies genetic alterations in pediatric low-grade gliomas.* Nature genetics, 2013. **45**(6): p. 602-612.

10. Jones, D.T.W., S. Kocialkowski, L. Liu, D.M. Pearson, L.M. Bäcklund, K. Ichimura et al., *Tandem duplication producing a novel oncogenic BRAF fusion gene defines the majority of pilocytic astrocytomas.* Cancer research, 2008. **68**(21): p. 8673-8677.

11. Schindler, G., D. Capper, J. Meyer, W. Janzarik, H. Omran, C. Herold-Mende et al., *Analysis of BRAF V600E mutation in 1,320 nervous system tumors reveals high mutation frequencies in pleomorphic xanthoastrocytoma, ganglioglioma and extra-cerebellar pilocytic astrocytoma.* Acta Neuropathologica, 2011. **121**(3): p. 397-405.

12. Banerjee, A., R.I. Jakacki, A. Onar-Thomas, S. Wu, T. Nicolaides, T. Young Poussaint et al., *A phase I trial of the MEK inhibitor selumetinib (AZD6244) in pediatric patients with recurrent or refractory low-grade glioma: a Pediatric Brain Tumor Consortium (PBTC) study.* Neuro-Oncology, 2017. **19**(8): p. 1135-1144.

13. McCowage, G.B., S. Mueller, C.A. Pratilas, D.R. Hargrave, C.L. Moertel, J. Whitlock et al., *Trametinib in pediatric patients with neurofibromatosis type 1 (NF-1)–associated plexiform neurofibroma: A phase I/IIa study.* 2018. **36**(15_suppl): p. 10504-10504.

14. Knight, T., M. Shatara, L. Carvalho, D. Altinok, J. Poulik, and Z.J. Wang, *Dramatic response to trametinib in a male child with neurofibromatosis type 1 and refractory astrocytoma.* Pediatr Blood Cancer, 2019. **66**(1): p. e27474.

15. Bouffet, E., M. Kieran, D. Hargrave, S. Roberts, I. Aerts, A. Broniscer et al., *LGG-46. TRAMETINIB THERAPY IN PEDIATRIC PATIENTS WITH LOW-GRADE GLIOMAS (LGG) WITH BRAF GENE FUSION; A DISEASE-SPECIFIC COHORT IN THE FIRST PEDIATRIC TESTING OF TRAMETINIB.* Neuro-Oncology, 2018. **20**(Suppl 2): p. i114-i114.

16. Cheng, Y. and H. Tian, *Current Development Status of MEK Inhibitors.* Molecules (Basel, Switzerland), 2017. **22**(10): p. 1551.

17. Agianian, B. and E. Gavathiotis, *Current Insights of BRAF Inhibitors in Cancer.* J Med Chem, 2018. **61**(14): p. 5775-5793.

18. Kidger, A.M., J. Sipthorp, and S.J. Cook, *ERK1/2 inhibitors: New weapons to inhibit the RAS-regulated RAF-MEK1/2-ERK1/2 pathway.* Pharmacol Ther, 2018. **187**: p. 45-60.

19. Keating, G.M. and A. Santoro, *Sorafenib.* Drugs, 2009. **69**(2): p. 223-240.

20. Karajannis, M.A., G. Legault, M.J. Fisher, S.S. Milla, K.J. Cohen, J.H. Wisoff et al., *Phase II study of sorafenib in children with recurrent or progressive low-grade astrocytomas.* Neuro Oncol, 2014. **16**(10): p. 1408-16.

21. Sievert, A.J., S.-S. Lang, K.L. Boucher, P.J. Madsen, E. Slaunwhite, N. Choudhari et al., *Paradoxical activation and RAF inhibitor resistance of BRAF protein kinase fusions characterizing pediatric astrocytomas.* Proceedings of the National Academy of Sciences of the United States of America, 2013. **110**(15): p. 5957-5962.

22. Selt, F., J. Hohloch, T. Hielscher, F. Sahm, D. Capper, A. Korshunov et al., *Establishment and application of a novel patient-derived KIAA1549:BRAF-driven pediatric pilocytic astrocytoma model for preclinical drug testing.* Oncotarget, 2017. **8**(7): p. 11460-11479.

23. Buhl, J.L., F. Selt, T. Hielscher, R. Guiho, J. Ecker, F. Sahm et al., *The senescence-associated secretory phenotype mediates oncogene-induced senescence in pediatric pilocytic astrocytoma.* Clinical Cancer Research, 2018: p. clincanres.1965.2018.

24. Stiles, C.D., G.T. Capone, C.D. Scher, H.N. Antoniades, J.J. Van Wyk, and W.J. Pledger, *Dual control of cell growth by somatomedins and platelet-derived growth factor.* Proceedings of the National Academy of Sciences of the United States of America, 1979. **76**(3): p. 1279-1283.

25. Kolb, E.A., R. Gorlick, P.J. Houghton, C.L. Morton, G. Neale, S.T. Keir et al., *Initial testing (stage 1) of AZD6244 (ARRY-142886) by the Pediatric Preclinical Testing Program.* Pediatr Blood Cancer, 2010. **55**(4): p. 668-77.

26. Schmitt, M. and M. Pawlita, *High-throughput detection and multiplex identification of cell contaminations.* Nucleic acids research, 2009. **37**(18): p. e119-e119.

27. Castro, F., W.G. Dirks, S. Fahnrich, A. Hotz-Wagenblatt, M. Pawlita, and M. Schmitt, *High-throughput SNP-based authentication of human cell lines.* Int J Cancer, 2013. **132**(2): p. 308-14.

28. Röring, M., R. Herr, G.J. Fiala, K. Heilmann, S. Braun, A.E. Eisenhardt et al., *Distinct requirement for an intact dimer interface in wild-type, V600E and kinase-dead B-Raf signalling.* The EMBO journal, 2012. **31**(11): p. 2629-2647.

29. Janknecht, R., W.H. Ernst, V. Pingoud, and A. Nordheim, *Activation of ternary complex factor Elk-1 by MAP kinases.* The EMBO journal, 1993. **12**(13): p. 5097-5104.

30. Weinberg, F., R. Griffin, M. Fröhlich, C. Heining, S. Braun, C. Spohr et al., *Identification and characterization of a BRAF fusion oncoprotein with retained autoinhibitory domains.* Oncogene, 2020. **39**(4): p. 814-832.

31. Ramurthy, S., B.R. Taft, R.J. Aversa, P.A. Barsanti, M.T. Burger, Y. Lou et al., *Design and Discovery of N-(3-(2-(2-Hydroxyethoxy)-6-morpholinopyridin-4-yl)-4-methylphenyl)-2-(trifluorom ethyl)isonicotinamide, a Selective, Efficacious, and Well-Tolerated RAF Inhibitor Targeting RAS Mutant Cancers: The Path to the Clinic.* J Med Chem, 2020. **63**(5): p. 2013-2027.

32. Bhagwat, S.V., W.T. McMillen, S. Cai, B. Zhao, M. Whitesell, W. Shen et al., *ERK Inhibitor LY3214996 Targets ERK Pathway-Driven Cancers: A Therapeutic Approach Toward Precision Medicine.* Mol Cancer Ther, 2020. **19**(2): p. 325-336.

33. Ecker, J., I. Oehme, R. Mazitschek, A. Korshunov, M. Kool, T. Hielscher et al., *Targeting class I histone deacetylase 2 in MYC amplified group 3 medulloblastoma.* Acta Neuropathol Commun, 2015. **3**: p. 22.

34. Chou, T.-C., *Drug Combination Studies and Their Synergy Quantification Using the Chou-Talalay Method.* Cancer Research, 2010: p. 0008-5472.CAN-09-1947.

35. Foucquier, J. and M. Guedj, *Analysis of drug combinations: current methodological landscape.* Pharmacology research & perspectives, 2015. **3**(3): p. e00149-e00149.

36. Miller, R.G., *Normal Univariate Techniques*, in *Simultaneous Statistical Inference*, R.G. Miller, Editor. 1981, Springer New York: New York, NY. p. 37-108.

37. Yandell, B., *Practical data analysis for designed experiments*. 2017: Routledge.

38. Caunt, C.J., M.J. Sale, P.D. Smith, and S.J. Cook, *MEK1 and MEK2 inhibitors and cancer therapy: the long and winding road.* Nature Reviews Cancer, 2015. **15**: p. 577.

39. Holderfield, M., T.E. Nagel, and D.D. Stuart, *Mechanism and consequences of RAF kinase activation by small-molecule inhibitors.* British Journal Of Cancer, 2014. **111**: p. 640.

40. Zhang, C., W. Spevak, Y. Zhang, E.A. Burton, Y. Ma, G. Habets et al., *RAF inhibitors that evade paradoxical MAPK pathway activation.* Nature, 2015. **526**: p. 583.

41. Le, K., E.S. Blomain, U. Rodeck, and A.E. Aplin, *Selective RAF inhibitor impairs ERK1/2 phosphorylation and growth in mutant NRAS, vemurafenib-resistant melanoma cells.* Pigment Cell Melanoma Res, 2013. **26**(4): p. 509-17.

42. *Phase I Study of LXH254 in Patients With Advanced Solid Tumors Haboring MAPK Pathway Alterations*. Available from: https://ClinicalTrials.gov/show/NCT02607813.

43. Peng, S.B., J.R. Henry, M.D. Kaufman, W.P. Lu, B.D. Smith, S. Vogeti et al., *Inhibition of RAF Isoforms and Active Dimers by LY3009120 Leads to Anti-tumor Activities in RAS or BRAF Mutant Cancers.* Cancer Cell, 2015. **28**(3): p. 384-98.

44. Hatzivassiliou, G., K. Song, I. Yen, B.J. Brandhuber, D.J. Anderson, R. Alvarado et al., *RAF inhibitors prime wild-type RAF to activate the MAPK pathway and enhance growth.* Nature, 2010. **464**: p. 431.

45. Shao, W., Y.M. Mishina, Y. Feng, G. Caponigro, V.G. Cooke, S. Rivera et al., *Antitumor Properties of RAF709, a Highly Selective and Potent Inhibitor of RAF Kinase Dimers, in Tumors Driven by Mutant RAS or BRAF.* Cancer Research, 2018. **78**(6): p. 1537.

46. Yin, N., W. Ma, J. Pei, Q. Ouyang, C. Tang, and L. Lai, *Synergistic and Antagonistic Drug Combinations Depend on Network Topology.* PLOS ONE, 2014. **9**(4): p. e93960.

47. Germann, U.A., B.F. Furey, W. Markland, R.R. Hoover, A.M. Aronov, J.J. Roix et al., *Targeting the MAPK Signaling Pathway in Cancer: Promising Preclinical Activity with the Novel Selective ERK1/2 Inhibitor BVD-523 (Ulixertinib).* Mol Cancer Ther, 2017. **16**(11): p. 2351-2363.

48. Gronych, J., A. Korshunov, J. Bageritz, T. Milde, M. Jugold, D. Hambardzumyan et al., *An activated mutant BRAF kinase domain is sufficient to induce pilocytic astrocytoma in mice.* J Clin Invest, 2011. **121**(4): p. 1344-8.

49. Raabe, E.H., K.S. Lim, J.M. Kim, A. Meeker, X.G. Mao, G. Nikkhah et al., *BRAF activation induces transformation and then senescence in human neural stem cells: a pilocytic astrocytoma model.* Clin Cancer Res, 2011. **17**(11): p. 3590-9.

50. Sun, Y., J.A. Alberta, C. Pilarz, D. Calligaris, E.J. Chadwick, S.H. Ramkissoon et al., *A brain-penetrant RAF dimer antagonist for the noncanonical BRAF oncoprotein of pediatric low-grade astrocytomas.* Neuro Oncol, 2017. **19**(6): p. 774-785.

51. Cheng, Z., D. Garvin, A. Paguio, P. Stecha, K. Wood, and F. Fan, *Luciferase Reporter Assay System for Deciphering GPCR Pathways.* Current chemical genomics, 2010. **4**: p. 84-91.

52. Zhang, R. and X. Xie, *Tools for GPCR drug discovery.* Acta Pharmacologica Sinica, 2012. **33**: p. 372.

53. Pratilas, C.A., B.S. Taylor, Q. Ye, A. Viale, C. Sander, D.B. Solit et al., *(V600E)BRAF is associated with disabled feedback inhibition of RAF-MEK signaling and elevated transcriptional output of the pathway.* Proc Natl Acad Sci U S A, 2009. **106**(11): p. 4519-24.

54. Karoulia, Z., E. Gavathiotis, and P.I. Poulikakos, *New perspectives for targeting RAF kinase in human cancer.* Nat Rev Cancer, 2017. **17**(11): p. 676-691.

55. Zhang, C., W. Spevak, Y. Zhang, E.A. Burton, Y. Ma, G. Habets et al., *RAF inhibitors that evade paradoxical MAPK pathway activation.* Nature, 2015. **526**(7574): p. 583-586.

56. Bollag, G., P. Hirth, J. Tsai, J. Zhang, P.N. Ibrahim, H. Cho et al., *Clinical efficacy of a RAF inhibitor needs broad target blockade in BRAF-mutant melanoma.* Nature, 2010. **467**(7315): p. 596-599.

57. Botton, T., E. Talevich, V.K. Mishra, T. Zhang, A.H. Shain, C. Berquet et al., *Genetic Heterogeneity of BRAF Fusion Kinases in Melanoma Affects Drug Responses.* Cell Rep, 2019. **29**(3): p. 573-588.e7.

58. Lito, P., A. Saborowski, J. Yue, M. Solomon, E. Joseph, S. Gadal et al., *Disruption of CRAF-mediated MEK activation is required for effective MEK inhibition in KRAS mutant tumors.* Cancer cell, 2014. **25**(5): p. 697-710.

59. Wang, J., Z. Yao, P. Jonsson, A.N. Allen, A.C.R. Qin, S. Uddin et al., *A secondary mutation in BRAF confers resistance to RAF inhibition in a BRAF V600E-mutant brain tumor.* Cancer Discovery, 2018: p. CD-17-1263.

60. Villanueva, J., J.R. Infante, C. Krepler, P. Reyes-Uribe, M. Samanta, H.-Y. Chen et al., *Concurrent MEK2 mutation and BRAF amplification confer resistance to BRAF and MEK inhibitors in melanoma.* Cell reports, 2013. **4**(6): p. 1090-1099.

61. Flaherty, K.T., J.R. Infante, A. Daud, R. Gonzalez, R.F. Kefford, J. Sosman et al., *Combined BRAF and MEK Inhibition in Melanoma with BRAF V600 Mutations.* New England Journal of Medicine, 2012. **367**(18): p. 1694-1703.

62. Whittaker, S.R., G.S. Cowley, S. Wagner, F. Luo, D.E. Root, and L.A. Garraway, *Combined Pan-RAF and MEK Inhibition Overcomes Multiple Resistance Mechanisms to Selective RAF Inhibitors.* Molecular Cancer Therapeutics, 2015. **14**(12): p. 2700-2711.

63. Merchant, M., J. Moffat, G. Schaefer, J. Chan, X. Wang, C. Orr et al., *Combined MEK and ERK inhibition overcomes therapy-mediated pathway reactivation in RAS mutant tumors.* PloS one, 2017. **12**(10): p. e0185862-e0185862.

815

Figure legends:

Figure 1: Generation of ELK-1 responsive reporter pediatric glioma cell lines: A) Schematic diagram of the plasmid pDIPZ (overview). ORI: Origin of replication; AmpR: Ampicillin resistance gene; LTR: Long terminal repeat; BlaR: Blasticidin resistance gene. Schematic diagram of the reporter gene cassette of the plasmids I) pDIPZ-CMV (ELK-1 binding site-CMV-desGFP-T2A-desFLuc) and III) pDIPZ-pFOS (ELK-1 binding site- pFOS-desGFP-T2A-desFLuc) and the plasmids without ELK-1 binding site II) pDIPZ-CMV w/o BS (CMV-desGFP-T2A-desFLuc) and IV) pDIPZ-pFOS w/o BS (pFOS-desGFP-T2A-desFLuc). desGFP: destablized GFP; desFLuc: destabilized firefly luciferase; w/o: without; BS: binding site. B) and C) Assessment of GFP positive cells after stable transduction of the reporter plasmids CMV (black) or pFOS (orange) pDIPZ in DKFZ-BT66 hTERT and BT-40 cells compared to cells without transduced plasmid. Fluorescence was determined by flow cytometry (Merck Guava EasyCyte HT). Depicted are mean +/- SD of three technical replicates.

Figure 2: Characterization of the ELK-1 responsive reporter assay signal: A) Comparison of bioluminescence (top row) (determined by Luciferase Assay System, Promega) versus fluorescence (bottom row) (determined by flow cytometry, Merck Guava EasyCyte HT) in DKFZ-BT66 hTERT and BT-40 cells both transduced with pDIPZ CMV (black) or pFOS (orange), after 24 hours of treatment with 1 µM trametinib or 1 µM vemurafenib, respectively. Depicted are mean +/- SD of three biological replicates. Significant differences are indicated as * $p<0.05$ and ** $p<0.01$. ns: not significant, $p>0.05$ (Student's t-test). B) Assessment of luminescence intensity measured by luciferase assay (Luciferase Assay System, Promega). DKFZ-BT66 hTERT and BT-40 cells, both transduced with either pDIPZ CMV or pFOS, were treated for 24 hours with trametinib in the indicated concentrations. Depicted are mean +/- SD of three biological replicates. p-values were calculated for the last values of each curve (treatment with highest concentration). ns: not significant, $p>0.05$ (Student's t-test). C) Assessment of absolute luminescence intensity using the luciferase assay (Steady-Glo® Luciferase Assay System) after treatment of DKFZ-BT66 hTERT or BT-40 cells both transduced with either pDIPZ CMV or pFOS with and without ELK-1 binding site with solvent or 1 µM trametinib for 24 hours. Depicted are mean +/- SD of three biological replicates. Significant differences are indicated as * $p<0.05$, ** $p<0.01$ and *** $p<0.001$. ns: not significant $p>0.05$ (Student's t-test). w/: with, w/o: without, native: cells without transduced plasmid. D) MAPK pathway activity in DKFZ-BT66 hTERT pDIPZ and BT-40 pDIPZ cells was determined by protein levels of pERK and ERK detected by Western blot after treatment with the indicated drugs for 24 hours with the same concentrations used in the luminescence assay in B) (every second concentration step).

Figure 3: Screening of a MAPK inhibitor library using the ELK-1 responsive reporter assay confirms ERK inhibitors followed by pan-RAF inhibitors as potential novel therapeutic approach for pLGGs: Heatmaps of tested MAPKi compounds ranked according to luminescence intensity (measured by Steady-Glo® Luciferase Assay System) after treatment for 24 hours in either DKFZ-BT66 pDIPZ-CMV A) or BT-40 pDIPZ-CMV cells B). Drug concentrations were used as indicated above the heatmap. Drugs were sorted by relative IC50 values with the lowest IC50 values at the top. n/a indicates that the IC50 value could not be estimated. In this case drugs were sorted by their ability to increase luminescence, thus paradoxically activating the MAPK pathway, from weak inducers at the top to strong inducers at the bottom. Pathway activity is depicted as follows: Green shades indicate pathway inhibition; blue shades no effect and red shades paradoxical activation. 1st, 2nd and 3rd describes the generation of each RAF inhibitor and I, I ½ and II their respective binding mode (adapted from [17, 32]). Depicted is the mean of three technical replicates. C) Boxplot of IC50 values assessed in DKFZ-BT66 and BT-40 cells drug screen combined for RAF, MEK and ERK inhibitors. Depicted are median (black bar), percentiles (25th to 75th) (box) and median +/- 1.5 IQR (interquartile range) (whiskers), and outliers (dots). Significant differences are indicated as * $p<0.05$. ns: not significant $p>0.05$ (Student's t-test, paired by drug).

Figure 4: Western blot validation of selected hits of the reporter screen: MAPK pathway activity in DKFZ-BT66 (+/-hTERT pDIPZ), BT-40 (+/-pDIPZ) and in MAPK pathway altered HEK293T cells was determined by protein levels of pERK and ERK detected by Western blot after treatment with the indicated drugs in the indicated concentrations for 24 hours. A) Comparison of MAPK pathway response after vemurafenib treatment. B) Treatment of DKFZ-BT66 cells with AZ628. C) Differential sensitivity to the treatment of PLX8394 in DKFZ-BT66 and BT-40 cells including quantification of pERK protein levels. D) Comparison of MAPK pathway response after PLX8294 treatment of MAPK pathway alteration expressing HEK293T cells and E) quantification of pMEK and pERK protein levels. Significant differences are indicated as * $p<0.05$, ** $p<0.01$ and *** $p<0.001$ (Tukey's 'Honest Significant Difference' test).

Figure 5: Analysis of MAPKi combination treatment in DKFZ-BT66 pDIPZ-CMV and BT-40 pDIPZ-CMV cells: A) Combination index (CI) tables for DKFZ-BT66 pDIPZ-CMV and BT-40 pDIPZ-CMV. Assessment of luminescence intensity measured by luciferase assay (Steady-Glo® Luciferase Assay System). CI values were calculated using CompuSyn. DKFZ-BT66 and BT-40 cells transduced with pDIPZ-CMV were treated for 24 hours with the indicated drugs and concentrations. Depicted are mean CI values of three biological replicates. Grey areas indicate experimental points which could not be included in the

CompuSyn analysis (fraction affected >1.0 or <0.0). B) Summary of combination index (CI) tables and isobolograms of MAPKi combination treatment in the *KIAA1549:BRAF* (DKFZ-BT66 pDIPZ-CMV) and $BRAF^{V600E}$ mutation (BT-40 pDIPZ-CMV) background. Heatmap includes median CI values obtained from the CI tables and CI values calculated for 0.5/0.75/0.9 fraction affected under MAPKi combination treatment. Fa: fraction affected.

Figure 6: Western blot validation of synergistic effects of selected combinations: MAPK pathway activity in A) DKFZ-BT66 and B) BT-40 cells was determined by protein levels of pERK, ERK, pRSK and RSK detected by Western blot after treatment with the indicated drugs in the indicated concentrations for 24 hours. Concentrations were chosen based on the isobologram of the respective combination (lanes of the Western blots: solvent, $Drug1_{IC90}$, $Drug2_{IC90}$, $Drug1_{Combi}$+$Drug2_{Combi}$ leading to 90% inhibition of the pathway, $Drug1_{Combi}$, $Drug2_{Combi}$). Combination index (CI) values were calculated using the Bliss independence model. Significant differences are indicated as * $p<0.05$, ** $p<0.01$ and *** $p<0.001$ (Tukey's 'Honest Significant Difference' test). Fa: Fraction affected, selu: selumetinib, dabra: dabrafenib.

Figure 1

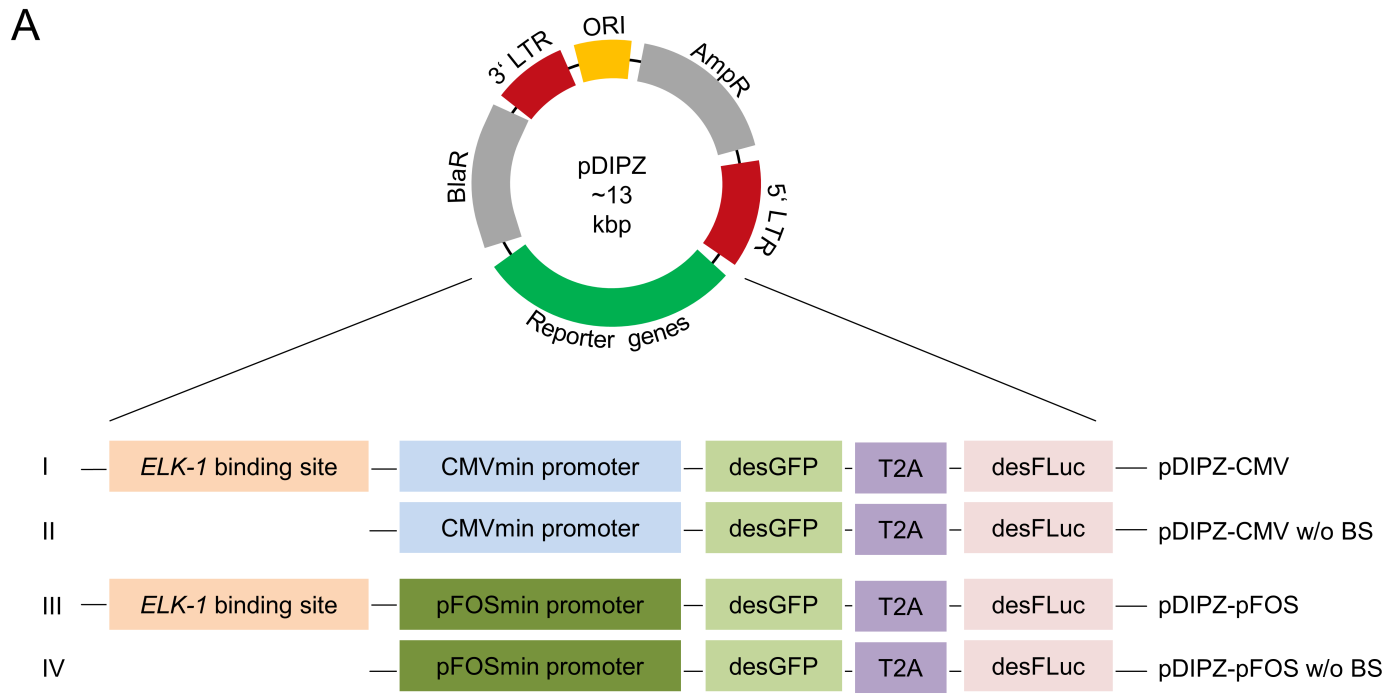
A
ORI
3' LTR
AmpR
BlaR
pDIPZ
~13
kbp
5' LTR
Reporter genes
I
ELK-1 binding site
CMVmin promoter
desGFP
T2A
desFLuc
pDIPZ-CMV
II
CMVmin promoter
desGFP
T2A
desFLuc
pDIPZ-CMV w/o BS
III
ELK-1 binding site
pFOSmin promoter
desGFP
T2A
desFLuc
pDIPZ-pFOS
IV
pFOSmin promoter
desGFP
T2A
desFLuc
pDIPZ-pFOS w/o BS

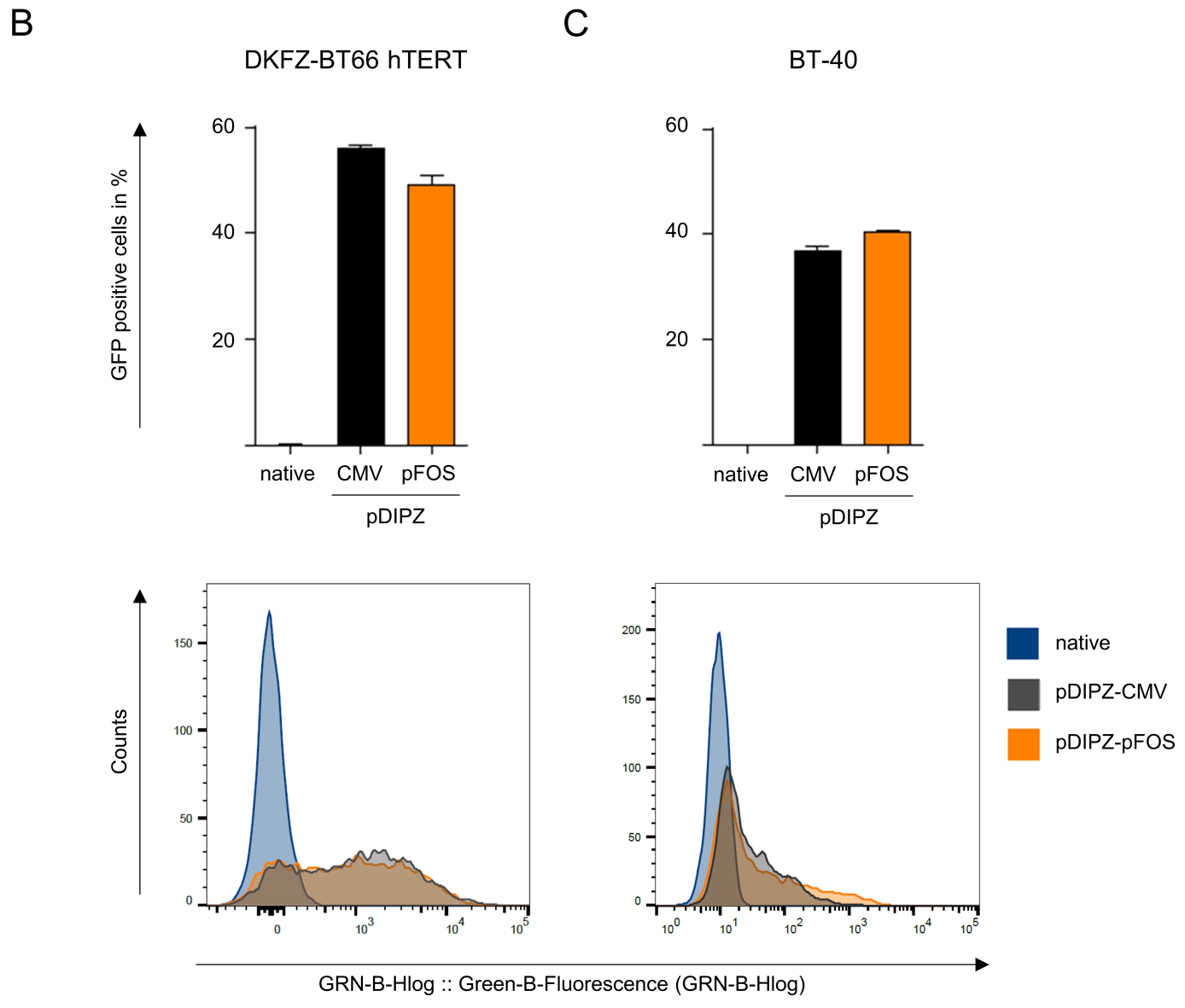
B
DKFZ-BT66 hTERT
GFP positive cells in %
60
40
20
native
CMV
pFOS
pDIPZ
C
BT-40
60
40
20
native
CMV
pFOS
pDIPZ
Counts
150
100
50
0
200
150
100
50
0
native
pDIPZ-CMV
pDIPZ-pFOS
GRN-B-Hlog :: Green-B-Fluorescence (GRN-B-Hlog)

Figure 2

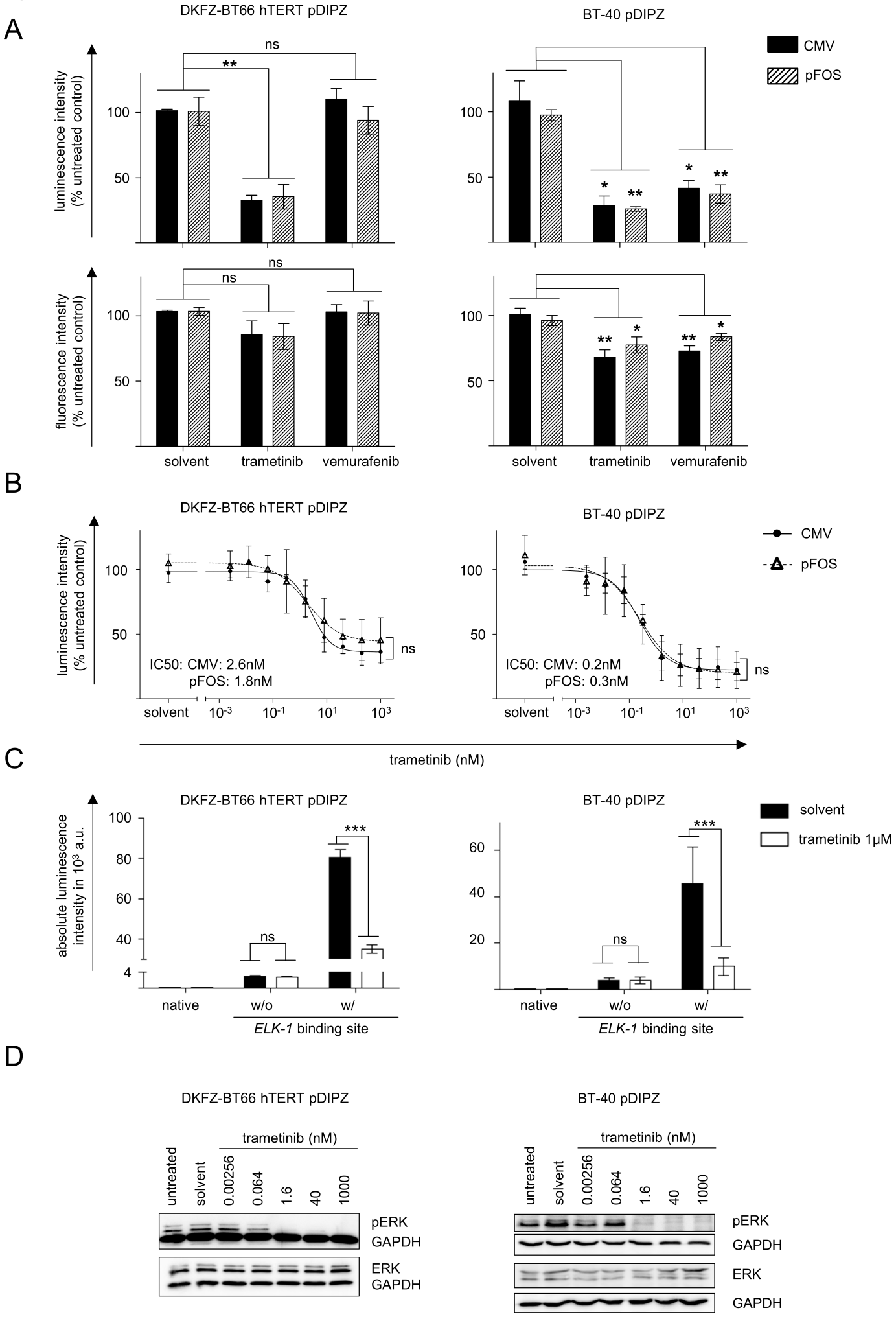
A
DKFZ-BT66 hTERT pDIPZ
BT-40 pDIPZ
CMV
pFOS
luminescence intensity (% untreated control)
fluorescence intensity (% untreated control)
ns
**
*
100
50
solvent
trametinib
vemurafenib
B
DKFZ-BT66 hTERT pDIPZ
BT-40 pDIPZ
CMV
pFOS
luminescence intensity (% untreated control)
IC50: CMV: 2.6nM
pFOS: 1.8nM
IC50: CMV: 0.2nM
pFOS: 0.3nM
solvent
10-3
10-1
101
103
trametinib (nM)
C
DKFZ-BT66 hTERT pDIPZ
BT-40 pDIPZ
solvent
trametinib 1µM
absolute luminescence intensity in 10³ a.u.
***
native
w/o
w/
ELK-1 binding site
D
DKFZ-BT66 hTERT pDIPZ
BT-40 pDIPZ
trametinib (nM)
untreated
solvent
0.00256
0.064
1.6
40
1000
pERK
GAPDH
ERK
GAPDH

Figure 3

A

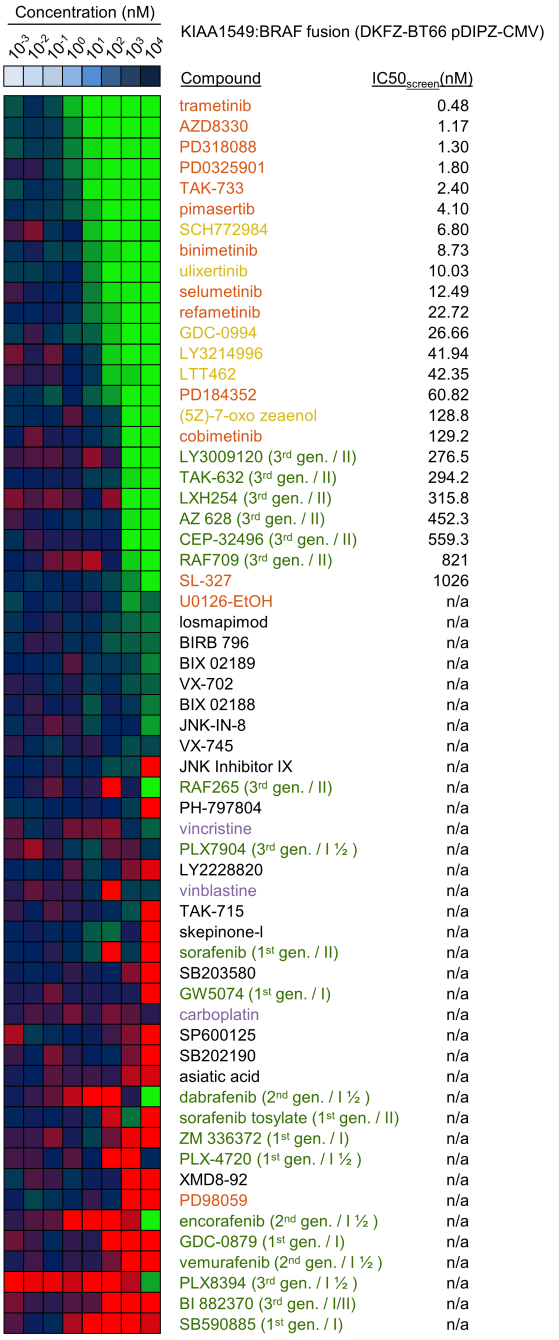
Concentration (nM)
10-3 10-2 10-1 100 101 102 103 104
KIAA1549:BRAF fusion (DKFZ-BT66 pDIPZ-CMV)
Compound IC50screen(nM)
trametinib 0.48
AZD8330 1.17
PD318088 1.30
PD0325901 1.80
TAK-733 2.40
pimasertib 4.10
SCH772984 6.80
binimetinib 8.73
ulixertinib 10.03
selumetinib 12.49
refametinib 22.72
GDC-0994 26.66
LY3214996 41.94
LTT462 42.35
PD184352 60.82
(5Z)-7-oxo zeaenol 128.8
cobimetinib 129.2
LY3009120 (3rd gen. / II) 276.5
TAK-632 (3rd gen. / II) 294.2
LXH254 (3rd gen. / II) 315.8
AZ 628 (3rd gen. / II) 452.3
CEP-32496 (3rd gen. / II) 559.3
RAF709 (3rd gen. / II) 821
SL-327 1026
U0126-EtOH n/a
losmapimod n/a
BIRB 796 n/a
BIX 02189 n/a
VX-702 n/a
BIX 02188 n/a
JNK-IN-8 n/a
VX-745 n/a
JNK Inhibitor IX n/a
RAF265 (3rd gen. / II) n/a
PH-797804 n/a
vincristine n/a
PLX7904 (3rd gen. / I ½) n/a
LY2228820 n/a
vinblastine n/a
TAK-715 n/a
skepinone-l n/a
sorafenib (1st gen. / II) n/a
SB203580 n/a
GW5074 (1st gen. / I) n/a
carboplatin n/a
SP600125 n/a
SB202190 n/a
asiatic acid n/a
dabrafenib (2nd gen. / I ½) n/a
sorafenib tosylate (1st gen. / II) n/a
ZM 336372 (1st gen. / I) n/a
PLX-4720 (1st gen. / I ½) n/a
XMD8-92 n/a
PD98059 n/a
encorafenib (2nd gen. / I ½) n/a
GDC-0879 (1st gen. / I) n/a
vemurafenib (2nd gen. / I ½) n/a
PLX8394 (3rd gen. / I ½) n/a
BI 882370 (3rd gen. / I/II) n/a
SB590885 (1st gen. / I) n/a

B

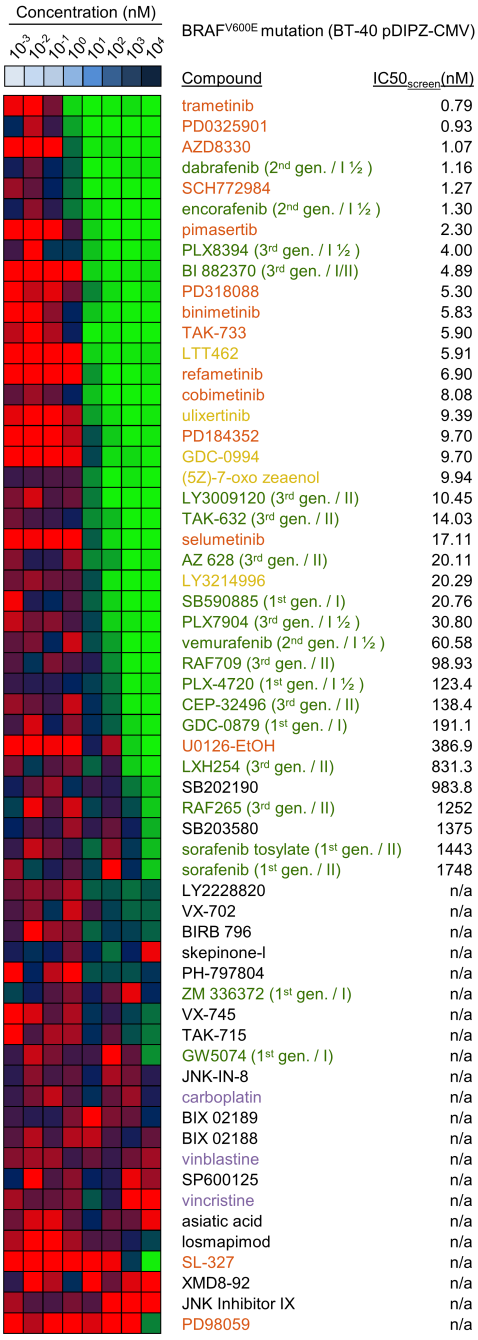
Concentration (nM)
10-3 10-2 10-1 100 101 102 103 104
BRAFV600E mutation (BT-40 pDIPZ-CMV)
Compound IC50screen(nM)
trametinib 0.79
PD0325901 0.93
AZD8330 1.07
dabrafenib (2nd gen. / I ½) 1.16
SCH772984 1.27
encorafenib (2nd gen. / I ½) 1.30
pimasertib 2.30
PLX8394 (3rd gen. / I ½) 4.00
BI 882370 (3rd gen. / I/II) 4.89
PD318088 5.30
binimetinib 5.83
TAK-733 5.90
LTT462 5.91
refametinib 6.90
cobimetinib 8.08
ulixertinib 9.39
PD184352 9.70
GDC-0994 9.70
(5Z)-7-oxo zeaenol 9.94
LY3009120 (3rd gen. / II) 10.45
TAK-632 (3rd gen. / II) 14.03
selumetinib 17.11
AZ 628 (3rd gen. / II) 20.11
LY3214996 20.29
SB590885 (1st gen. / I) 20.76
PLX7904 (3rd gen. / I ½) 30.80
vemurafenib (2nd gen. / I ½) 60.58
RAF709 (3rd gen. / II) 98.93
PLX-4720 (1st gen. / I ½) 123.4
CEP-32496 (3rd gen. / II) 138.4
GDC-0879 (1st gen. / I) 191.1
U0126-EtOH 386.9
LXH254 (3rd gen. / II) 831.3
SB202190 983.8
RAF265 (3rd gen. / II) 1252
SB203580 1375
sorafenib tosylate (1st gen. / II) 1443
sorafenib (1st gen. / II) 1748
LY2228820 n/a
VX-702 n/a
BIRB 796 n/a
skepinone-l n/a
PH-797804 n/a
ZM 336372 (1st gen. / I) n/a
VX-745 n/a
TAK-715 n/a
GW5074 (1st gen. / I) n/a
JNK-IN-8 n/a
carboplatin n/a
BIX 02189 n/a
BIX 02188 n/a
vinblastine n/a
SP600125 n/a
vincristine n/a
asiatic acid n/a
losmapimod n/a
SL-327 n/a
XMD8-92 n/a
JNK Inhibitor IX n/a
PD98059 n/a

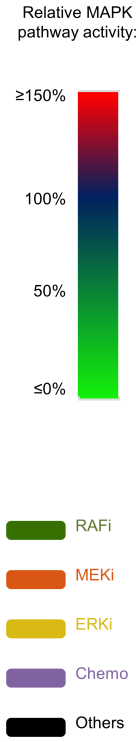
Relative MAPK pathway activity:
≥150%
100%
50%
≤0%
RAFi
MEKi
ERKi
Chemo
Others

C

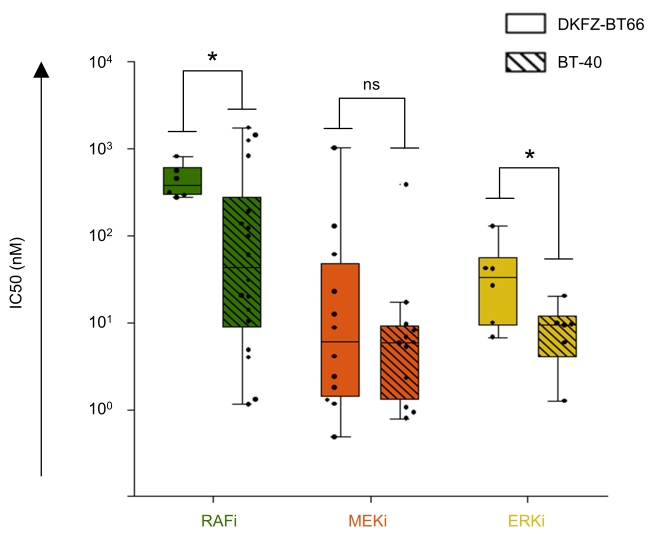
DKFZ-BT66
BT-40
IC50 (nM)
10^4
10^3
10^2
10^1
10^0
*
ns
*
RAFi
MEKi
ERKi

Figure 4

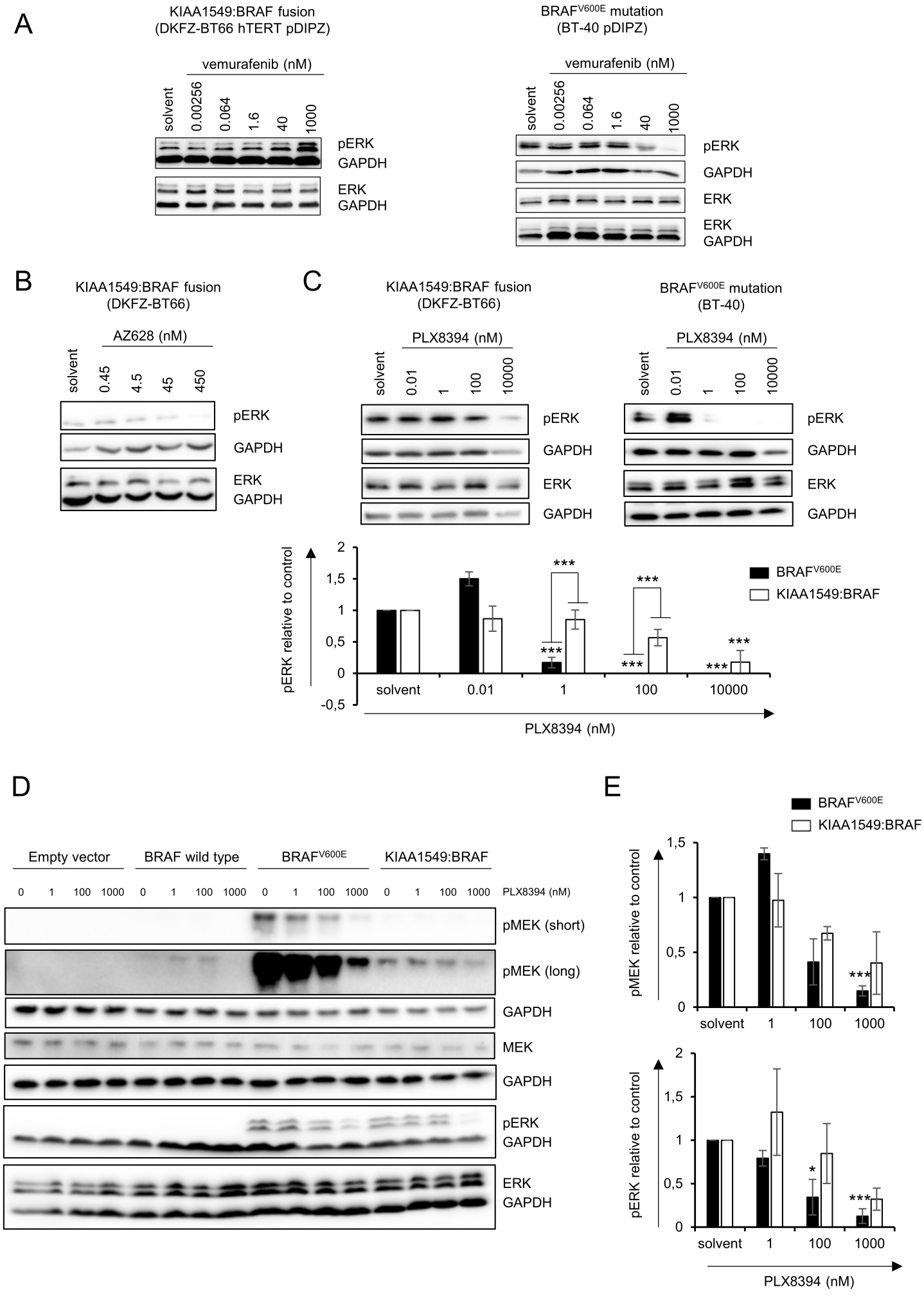
A
KIAA1549:BRAF fusion
(DKFZ-BT66 hTERT pDIPZ)
vemurafenib (nM)
solvent
0.00256
0.064
1.6
40
1000
pERK
GAPDH
ERK
GAPDH
BRAFV600E mutation
(BT-40 pDIPZ)
vemurafenib (nM)
solvent
0.00256
0.064
1.6
40
1000
pERK
GAPDH
ERK
GAPDH
B
KIAA1549:BRAF fusion
(DKFZ-BT66)
AZ628 (nM)
solvent
0.45
4.5
45
450
pERK
GAPDH
ERK
GAPDH
C
KIAA1549:BRAF fusion
(DKFZ-BT66)
PLX8394 (nM)
solvent
0.01
1
100
10000
pERK
GAPDH
ERK
GAPDH
BRAFV600E mutation
(BT-40)
PLX8394 (nM)
solvent
0.01
1
100
10000
pERK
GAPDH
ERK
GAPDH
pERK relative to control
2
1,5
1
0,5
0
-0,5
***
solvent
0.01
1
100
10000
PLX8394 (nM)
BRAFV600E
KIAA1549:BRAF
D
Empty vector
BRAF wild type
BRAFV600E
KIAA1549:BRAF
0 1 100 1000 0 1 100 1000 0 1 100 1000 0 1 100 1000
PLX8394 (nM)
pMEK (short)
pMEK (long)
GAPDH
MEK
GAPDH
pERK
GAPDH
ERK
GAPDH
E
BRAFV600E
KIAA1549:BRAF
pMEK relative to control
1,5
1
0,5
0
***
solvent
1
100
1000
pERK relative to control
2
1,5
1
0,5
0
*
***
solvent
1
100
1000
PLX8394 (nM)

Figure 5

A

KIAA1549:BRAF fusion (DKFZ-BT66 pDIPZ-CMV)

BRAF^{V600E} mutation (BT-40 pDIPZ-CMV)

RAFi + MEKi

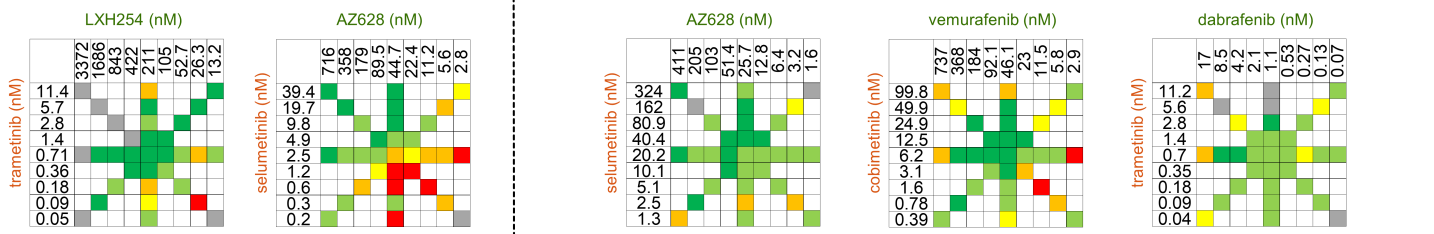

RAFi + ERKi

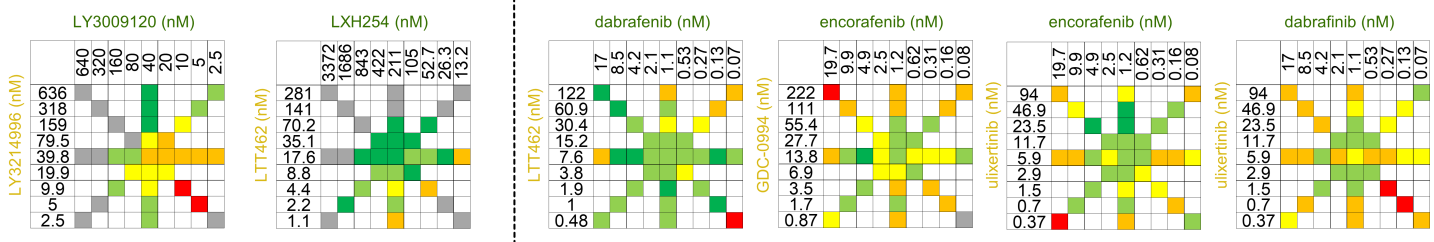

MEKi + ERKi

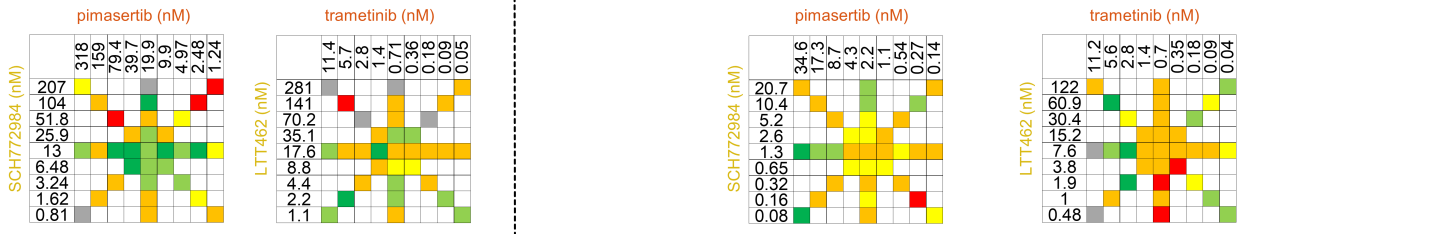

B

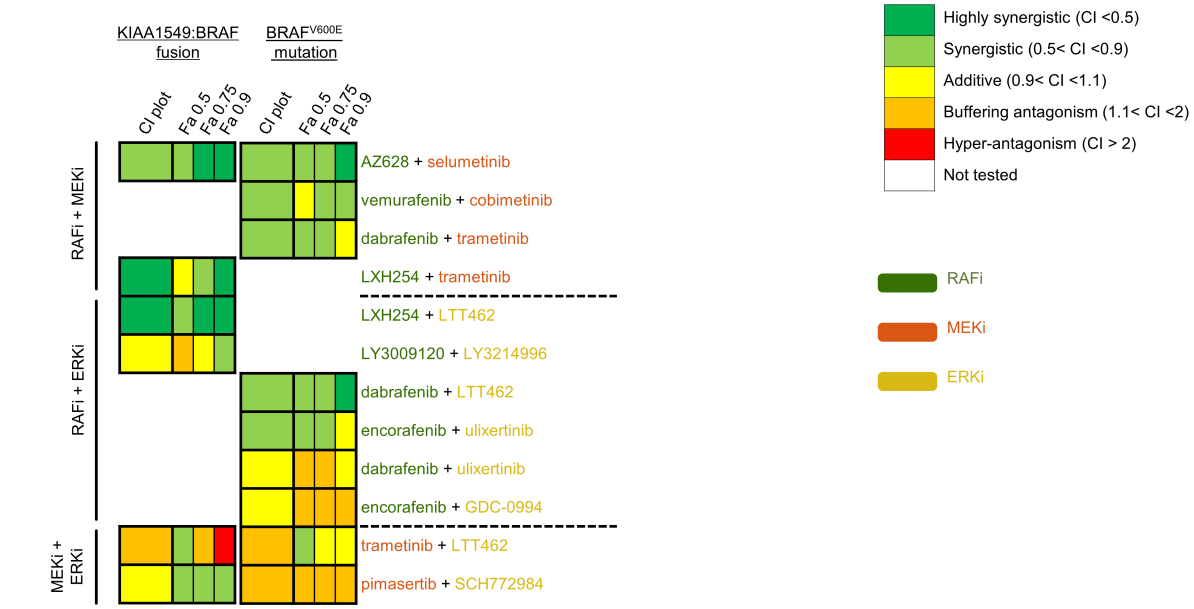

Figure 6

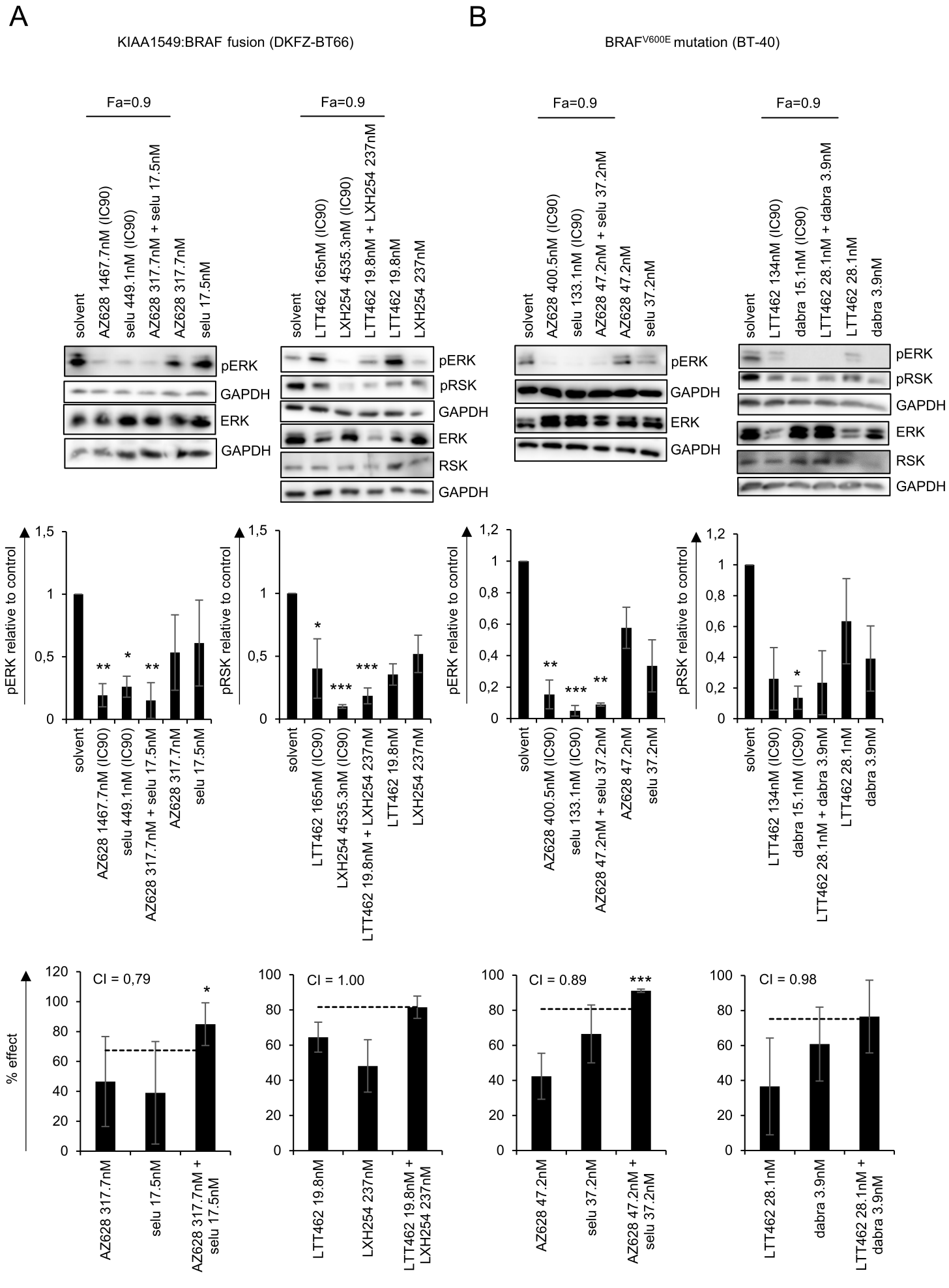
A
KIAA1549:BRAF fusion (DKFZ-BT66)
B
BRAF V600E mutation (BT-40)
Fa=0.9
solvent
AZ628 1467.7nM (IC90)
selu 449.1nM (IC90)
AZ628 317.7nM + selu 17.5nM
AZ628 317.7nM
selu 17.5nM
LTT462 165nM (IC90)
LXH254 4535.3nM (IC90)
LTT462 19.8nM + LXH254 237nM
LTT462 19.8nM
LXH254 237nM
AZ628 400.5nM (IC90)
selu 133.1nM (IC90)
AZ628 47.2nM + selu 37.2nM
AZ628 47.2nM
selu 37.2nM
LTT462 134nM (IC90)
dabra 15.1nM (IC90)
LTT462 28.1nM + dabra 3.9nM
LTT462 28.1nM
dabra 3.9nM
pERK
pRSK
GAPDH
ERK
RSK
pERK relative to control
pRSK relative to control
% effect
CI = 0,79
CI = 1.00
CI = 0.89
CI = 0.98